Coronal Condensations in Hybrid Prominence/Coronal Rain Structures

Leping Li

lepingli@nao.cas.cn

National Astronomical Observatories (NAO)

Chinese Academy of Sciences (CAS)

Outline

1. Introduction

2. Coronal condensation (**CC**) facilitated by magnetic reconnection (**MR**) between open and closed magnetic structures (Li+ 2018a, 2018b, 2019, 2020, 2021a, 2021b, 2021c, Chen+ 2022)

3. Summary

1. Introduction

- **CC** of cool plasma out of the hot corona is widely investigated, best seen at the solar limb. (see reviews in Antolin 2020 and Antolin & Froment 2021, and references therein)
- **CC** is based on the thermal properties of the plasma alone. Only the loss of thermal equilibrium between heat input, heat conduction, and radiative losses causes the plasma to cool catastrophically. (Müller+ 2003, Xia & Keppens 2016, et al.)
- **CC** is independent of the (evolution of the) coronal magnetic field.
- Solar activities, closely associated with **CC**, include the prominence and coronal rain (**CR**).

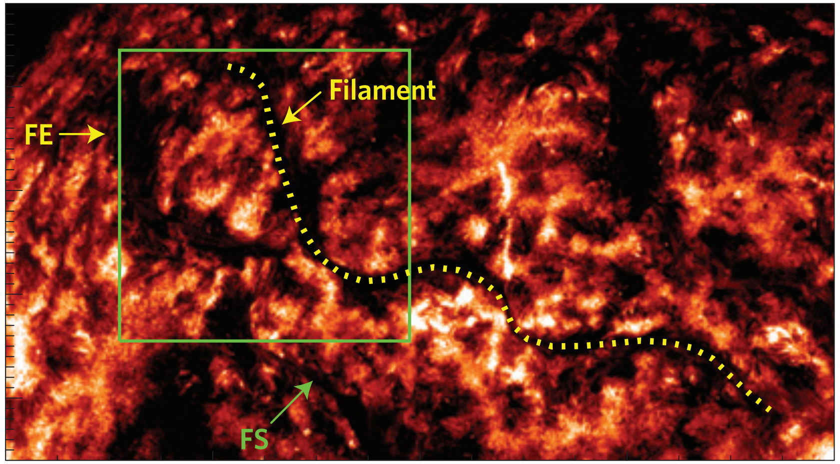

Li+ 2016, Nature Physics, 12, 847

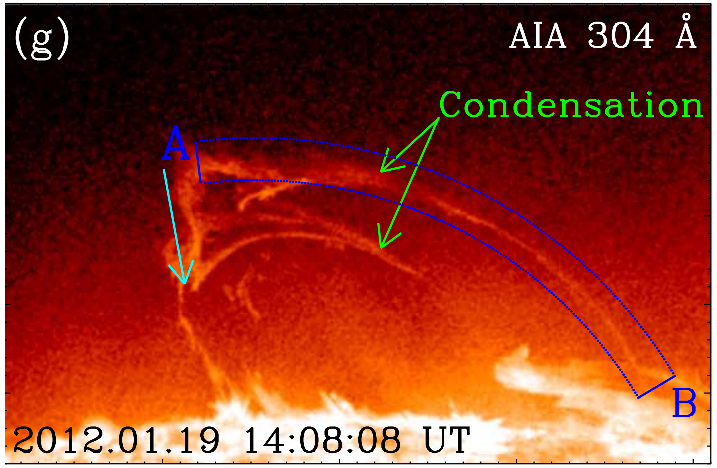

Li+ 2018a, ApJL, 864, L4

MR

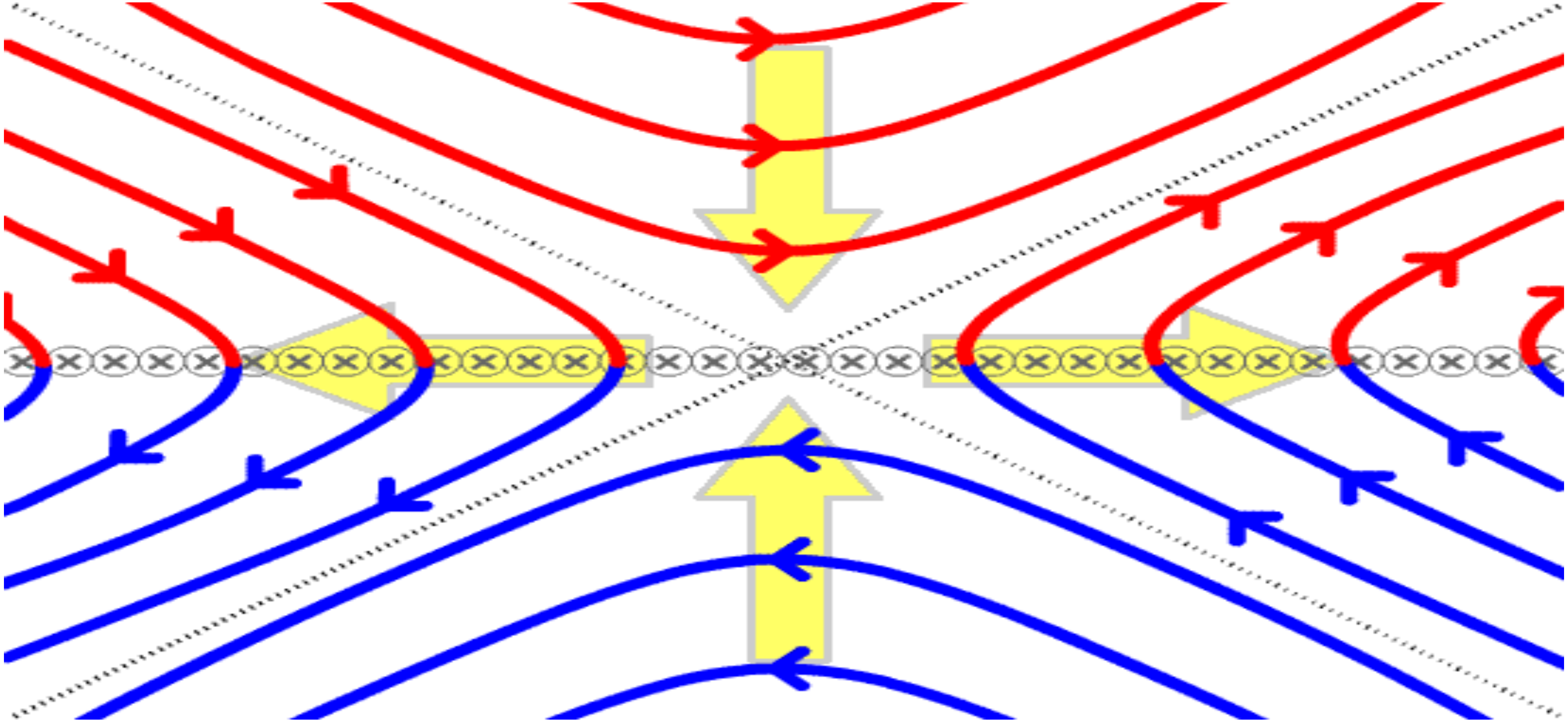

- **MR** shows the reconfiguration of magnetic field geometry.
- It is used to explain the rapid release of magnetic energy, and its conversion to other forms, e.g., thermal and kinetic. (Priest & Forbes 2000, Lin & Forbes 2000)

Formation of Prominences

- Prominence formation includes the formation of (1) **magnetic structure** and (2) **mass** of prominences, respectively.

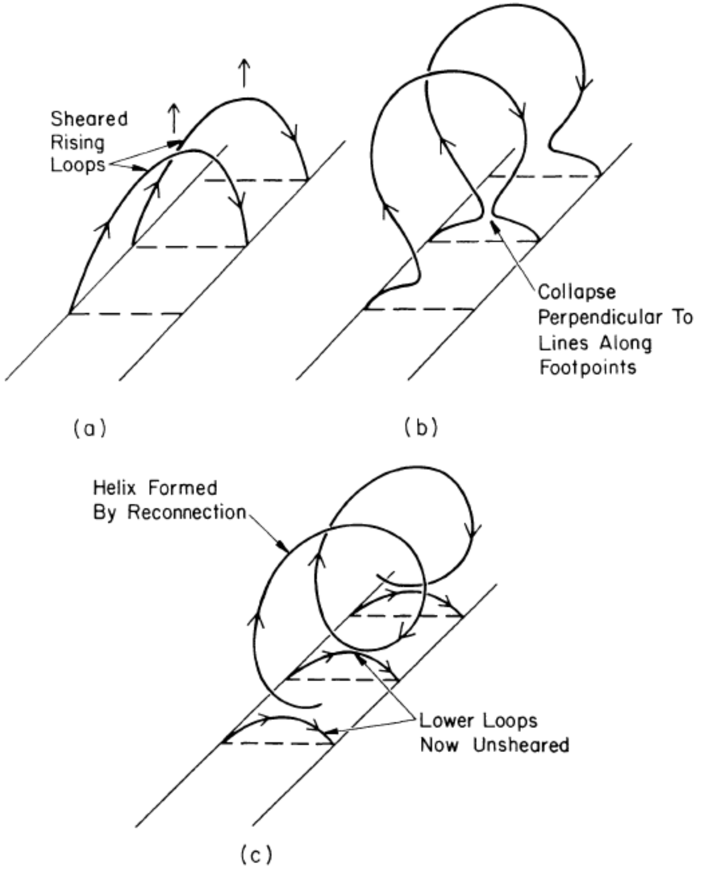

Pneuman (1983)

- **MR** causes a helical magnetic structure with numerous dips of prominences. (Pneuman 1983, van Ballegooijen & Martens 1989, et al.)

- **CC** of hot plasma trapped in the helices forms the mass of prominences. (Pneuman 1983, Xia+ 2014, et al.)

Coronal Cloud Prominences

- Coronal cloud prominences, also referred to as "Coronal spiders" and "funnel prominences". (Liu+ 2012, Vial & Engvold 2015)

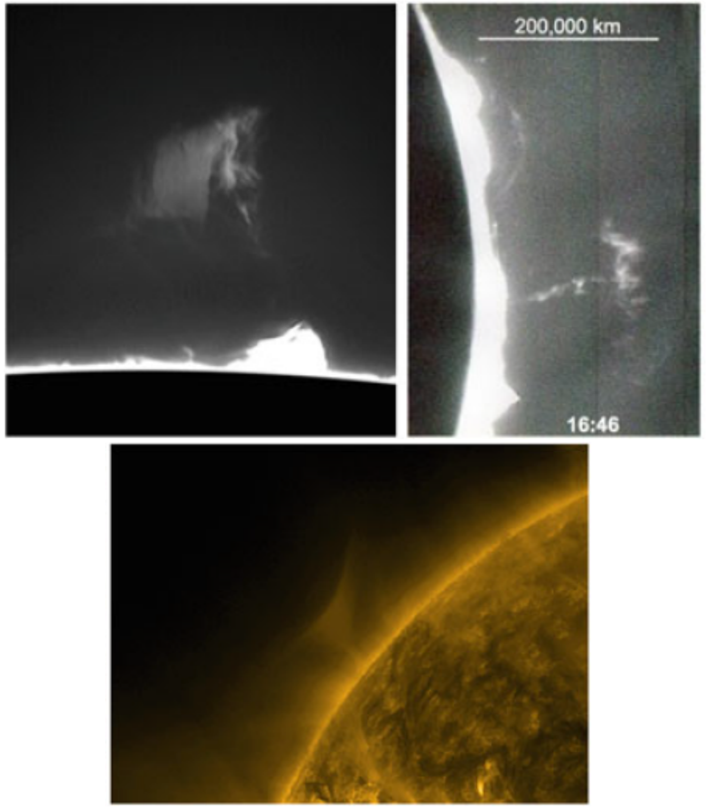

Table 9.1 Comparison of channel prominences with coronal cloud prominences

Channel prominences with spine and barbs	Coronal cloud prominences often above invisible arcs
Low < 50,000 km	High (up to ~200,000 km)
Bright (1,011 particles/cc)	Faint ($\sim 10^{10}$ particles/cc)
Seen against disk in Hα	Rarely seen against disk in Hα
Reveal counterstreaming in spine and barbs	Only down flows from unknown sources
Located in filament channels	Not in filament channels
Mass input from injection sites where magnetic fields are cancelling	Mass input from previously ejected filament mass or CME's—two of several hypotheses
Lie above polarity reversal boundaries in filament channels	Might lie within coronal loop systems above separatrix surfaces
Have chirality (handedness)	No known chirality (handedness)
Often end lifetime by erupting with a CME	Rarely erupt; large ones form after a CME with an erupting filament

Vail & Engvold (2015)

- They differ from the common, channel prominences in several aspects, and disappear from drainage along curved trajectories resembling **CR**.
- The formation process is not fully understood.

Two Types of CR

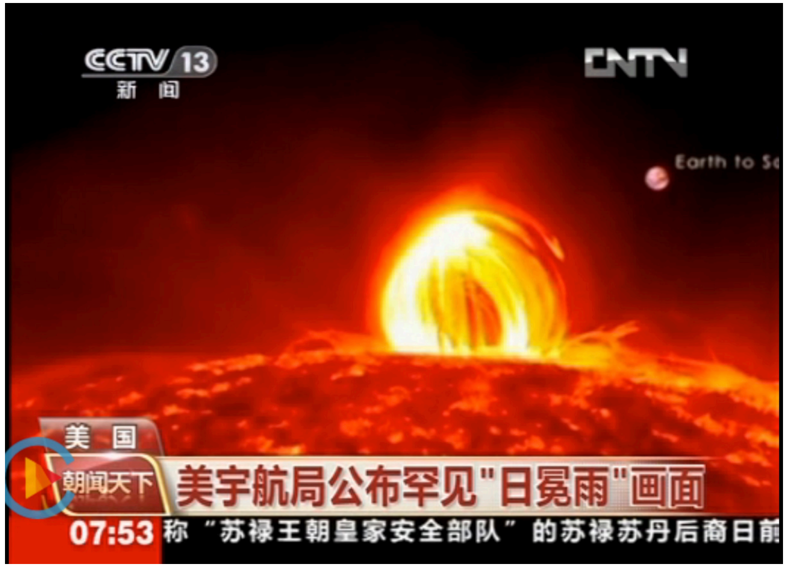

Flare-driven post-flare **CR**

Thermal conduction front/beamed nonthermal particles

=> chromospheric evaporation

=> thermal non-equlibrium => **CC** => **CR**

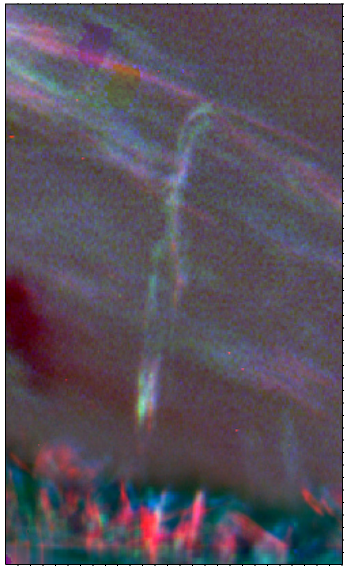

Antolin+ (2015)

Non-flare driven active region **CR**

Heating at/around the loop endpoints

=> chromospheric evaporation

=> thermal instability => **CC** => **CR**

- Both **CR**s occur along magnetically-closed field lines;
- Magnetic field evolution and thermal evolution are treated separately for both formation mechanisms of the prominences and **CR**s.

- The magnetic and thermal evolution has to be treated together and cannot be separated, even in the case of catastrophic cooling. (Li+ 2018a, 2018b, 2019, 2020, 2021a, 2021b, 2021c, Chen+ 2022)

2.1 MR-CC between Open and Closed Structures

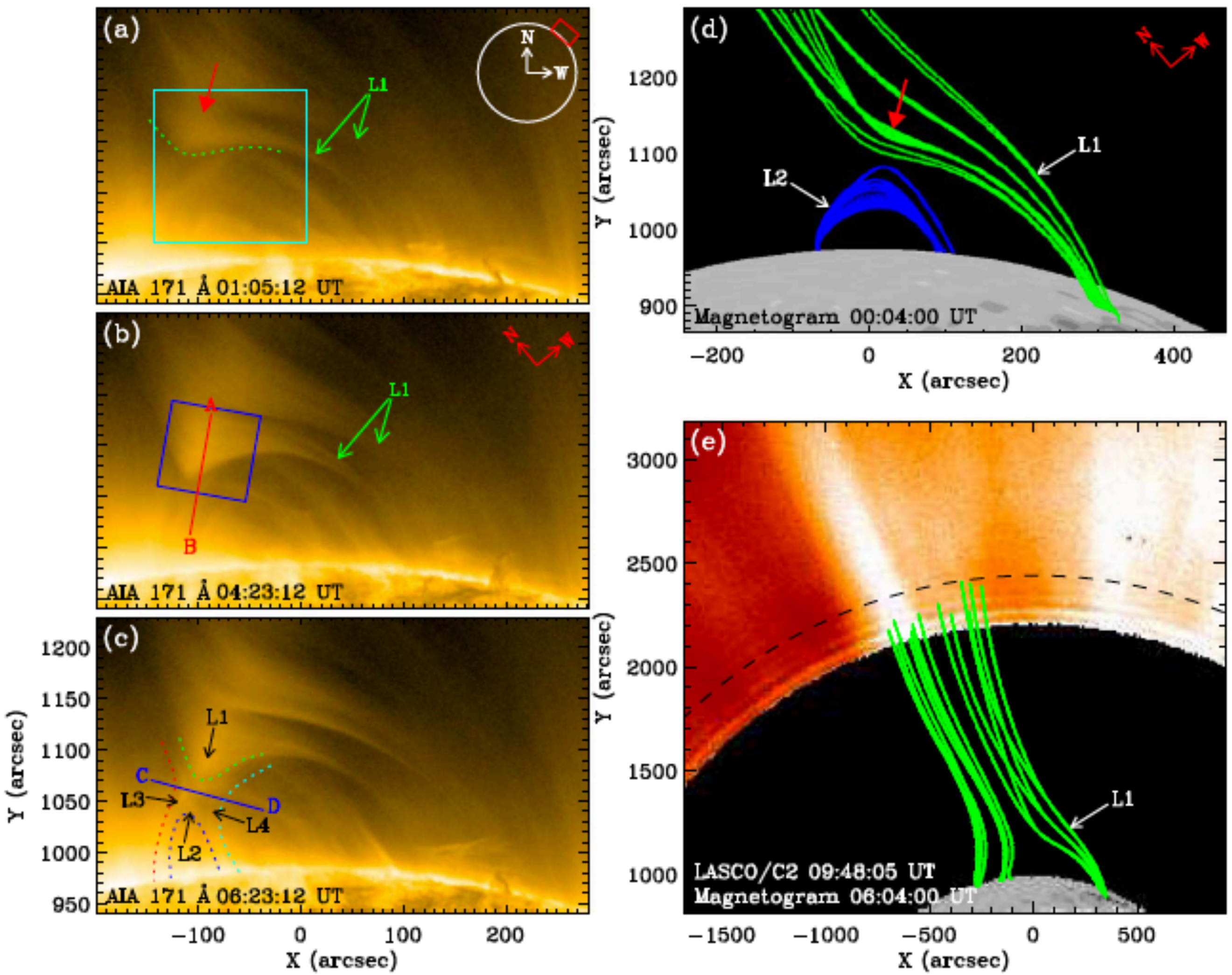

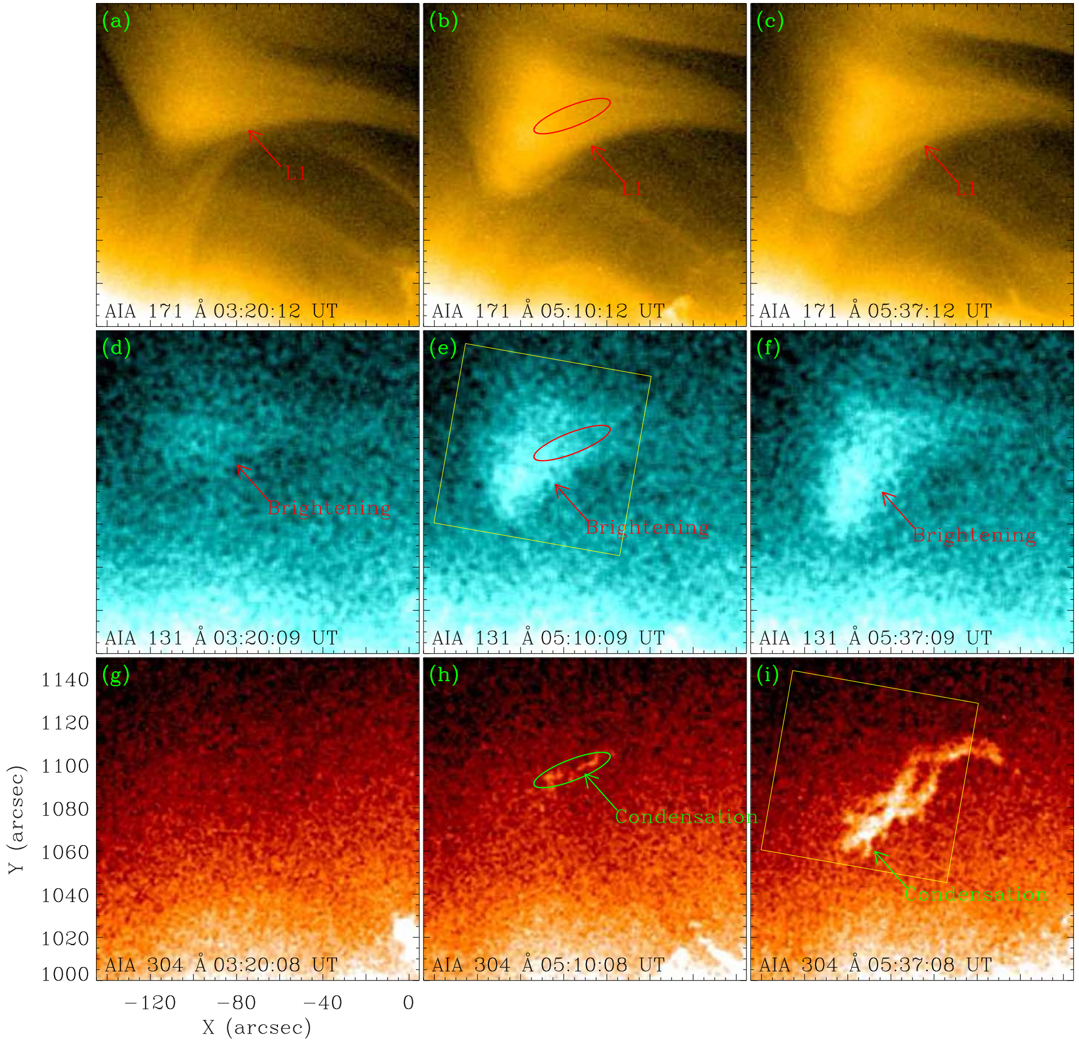

MR between open and closed structures, and **CC** as a coronal cloud prominence (Li+ 2018a, ApJ, 864, L4)

CC and Its Downflows As CR

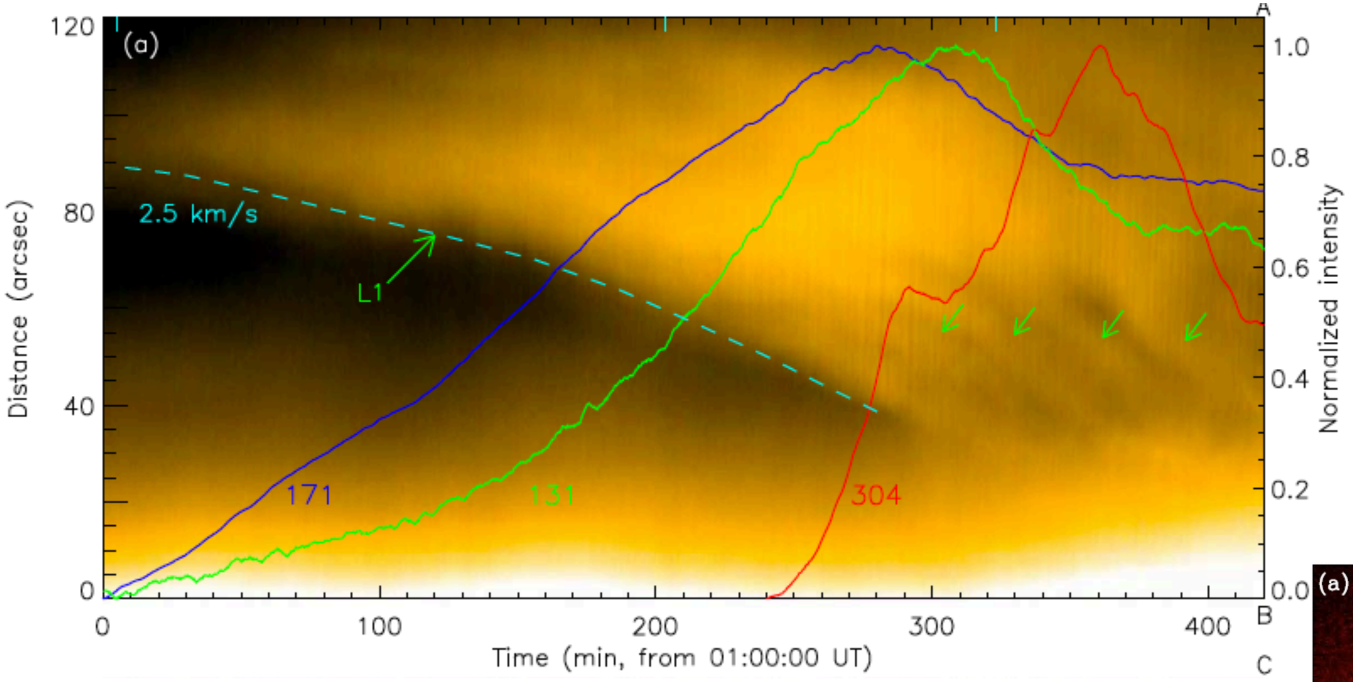

Blue, green, and red lightcurves show the cooling and **CC** of coronal plasma.

Downflows of **CC** as **CR**

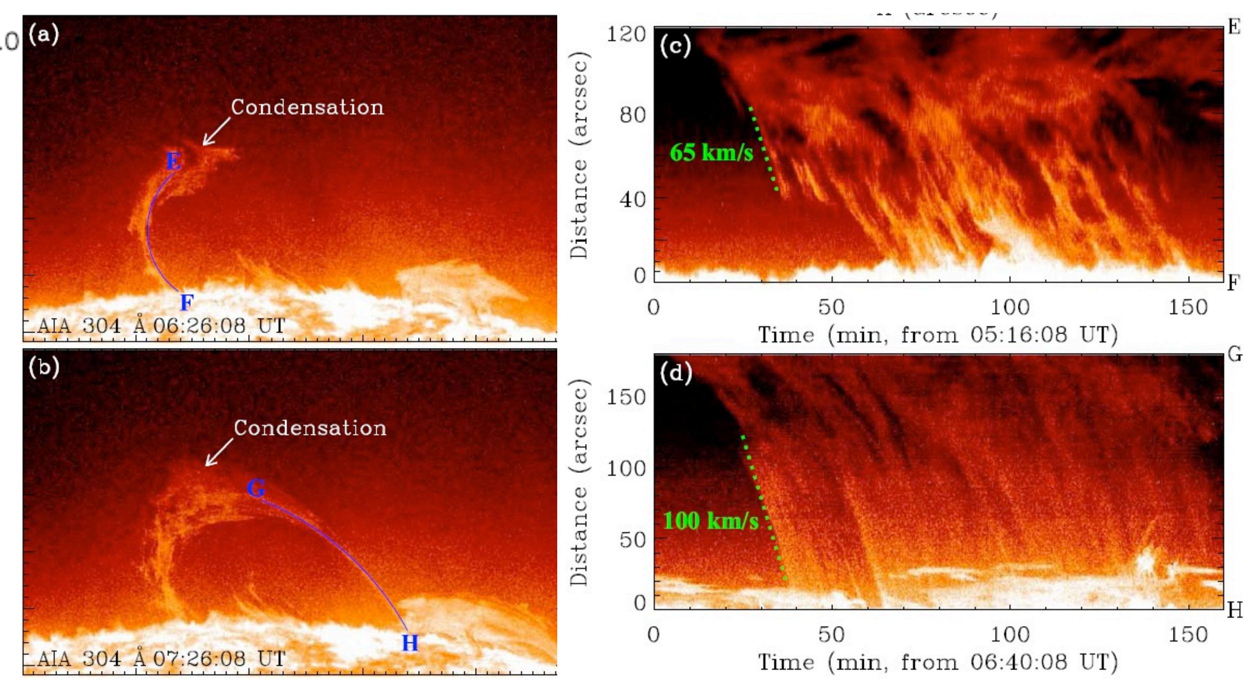

Schematic Diagrams of MR-CC

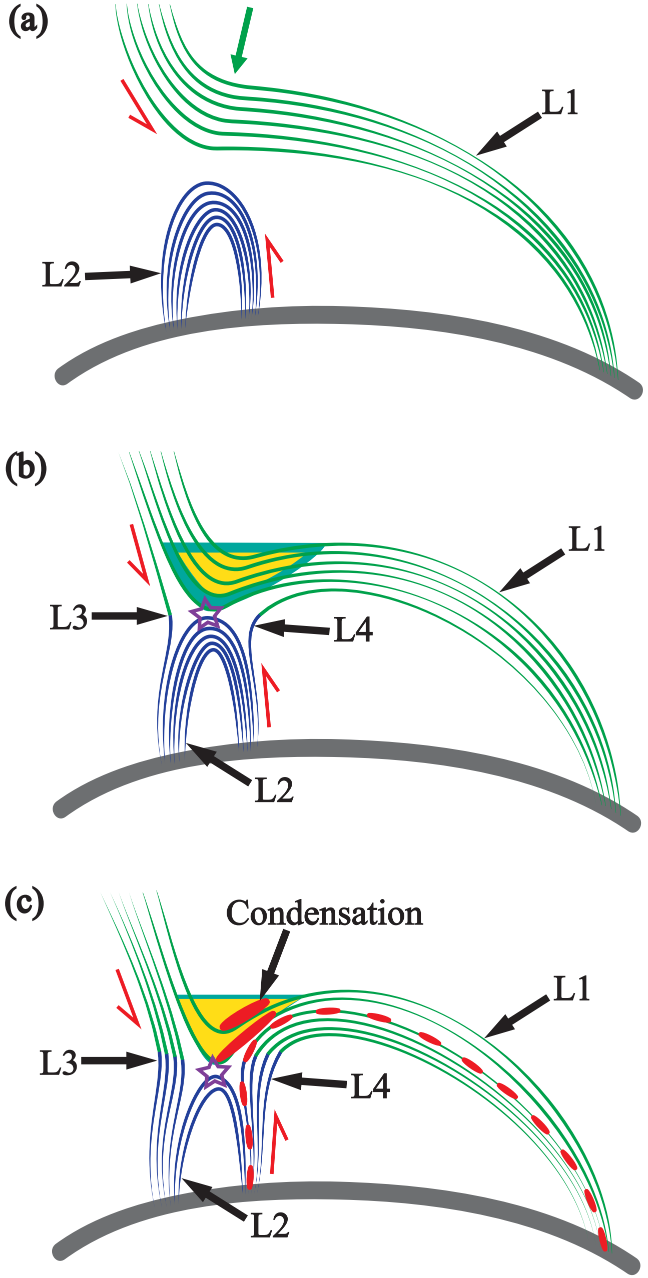

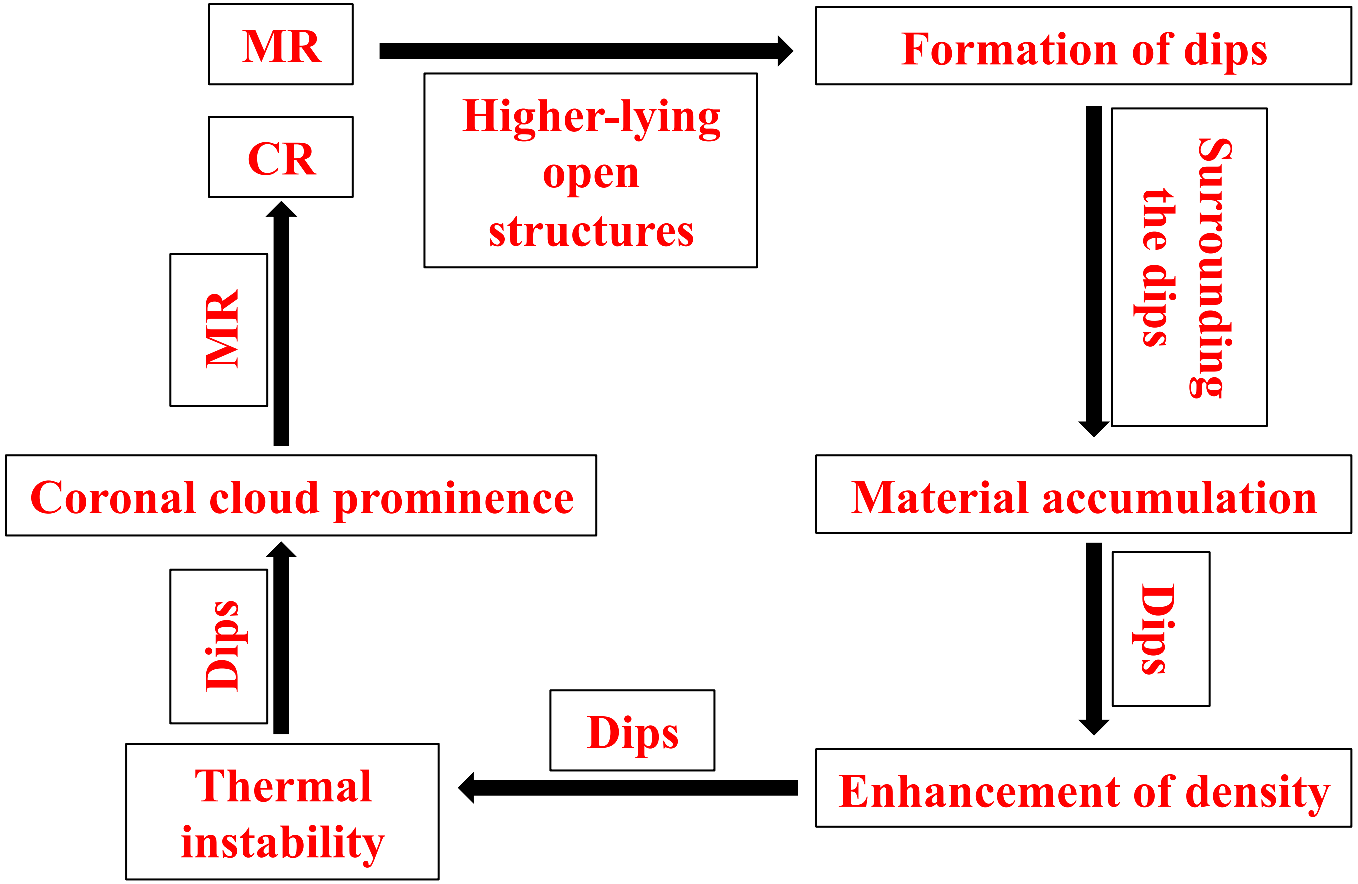

- **MR** thus plays an important role in the mass cycle of coronal plasma.
- A new and alternative mechanism for the formation of **CR** along open field lines through **MR** is suggested, away from those along closed field lines.

2.2 Quasi-periodic Fast Propagating Magnetoacoustic Waves during MR-CC

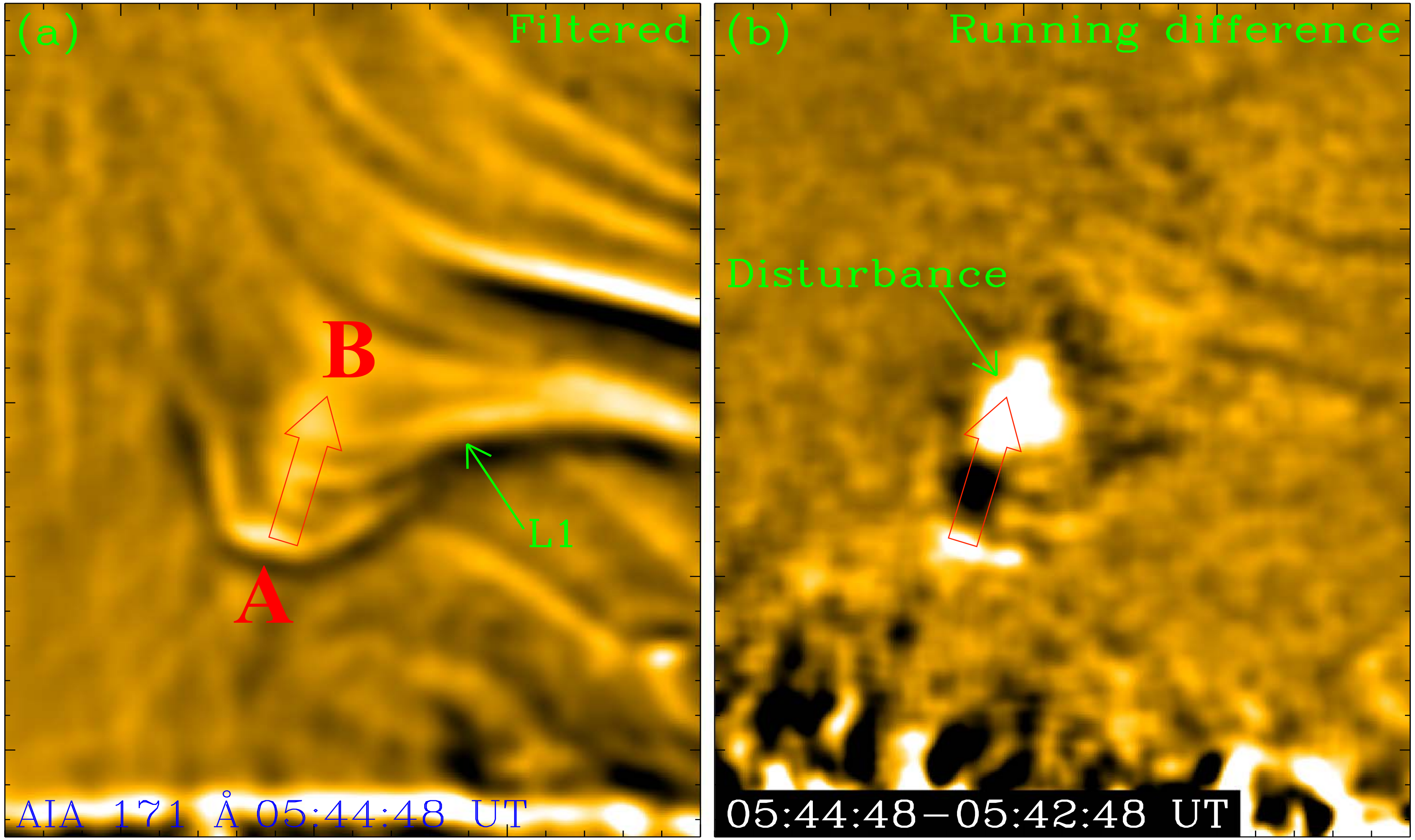

- Disturbances, originating from the **MR** region, propagate upward across the dip region of loops L1 (Li+ 2018b, ApJ, 868, L33).

Propagating Disturbances

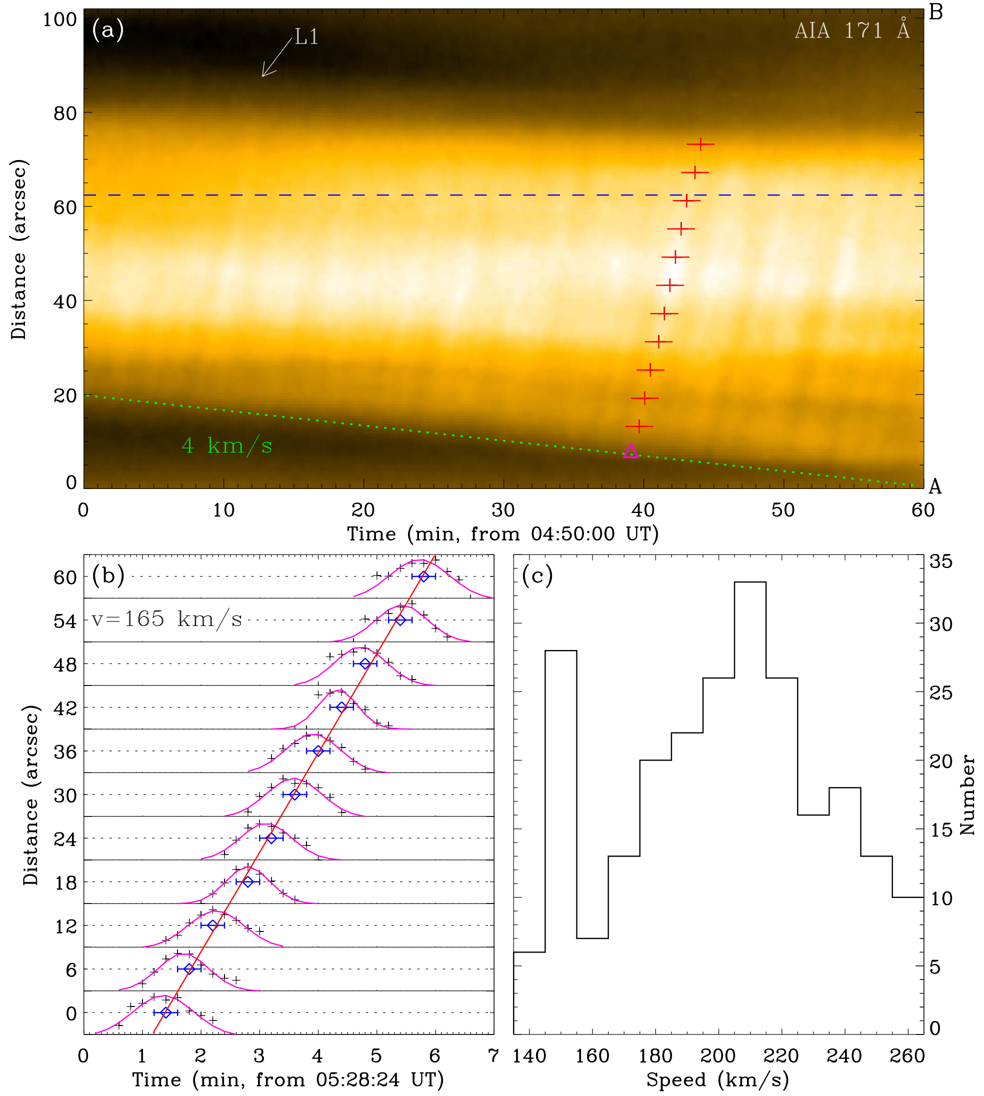

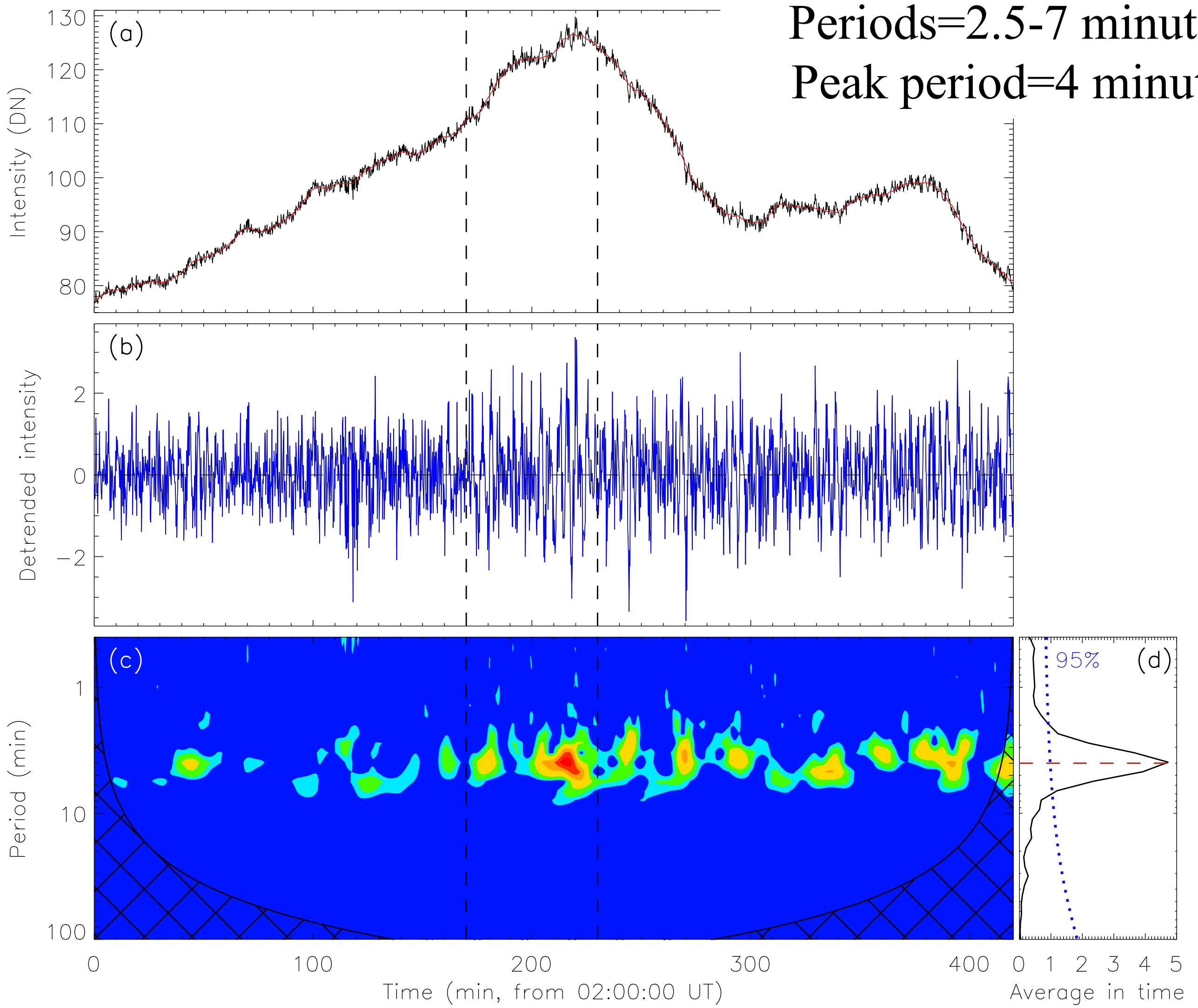

Periods=2.5-7 minutes;
Peak period=4 minutes

- The disturbances represent the fast-propagating magnetoacoustic waves.
- Magnetic energy is mainly converted into wave energy by **MR**.

2.3 Repeated MR-CC Events

Table 1
General Information on Repeated Coronal Condensations and MRs between Loops from 2012 January 16 to 20

Event	Section	Start Time	End Time	AIA Emission			EUVI-A Emission	
				171 Å	131 Å	304 Å	171 Å	304 Å
1	3.1	Jan 16 04:00 UT	Jan 16 20:00 UT	Yes	Yes	No	Yes	No
2	3.2	Jan 16 20:30 UT	Jan 17 04:30 UT	Yes	Yes	Yes	Yes	Yes
3	3.3	Jan 17 07:00 UT	Jan 17 22:00 UT	Yes	Yes	Yes	Yes	Yes
4	A	Jan 17 22:00 UT	Jan 18 10:00 UT	Yes	Yes	Yes	Yes	Yes
5	B	Jan 19 01:00 UT	Jan 20 02:30 UT	Yes	Yes	Yes	No	No
6	C	Jan 20 03:00 UT	Jan 21 03:00 UT	Yes	Yes	Yes	No	No

- From the same magnetic structure system, in 5 days, 15 similar **MR-CC** events occur repeatedly.
- Coronal cloud prominences thus form.
- The **CC** remains for 30 min to 15 hr, and then rain down to the chromosphere as **CR**. (Li+ 2019, ApJ, 884, 34)

An Example: The 6th Event on 2012 January 20

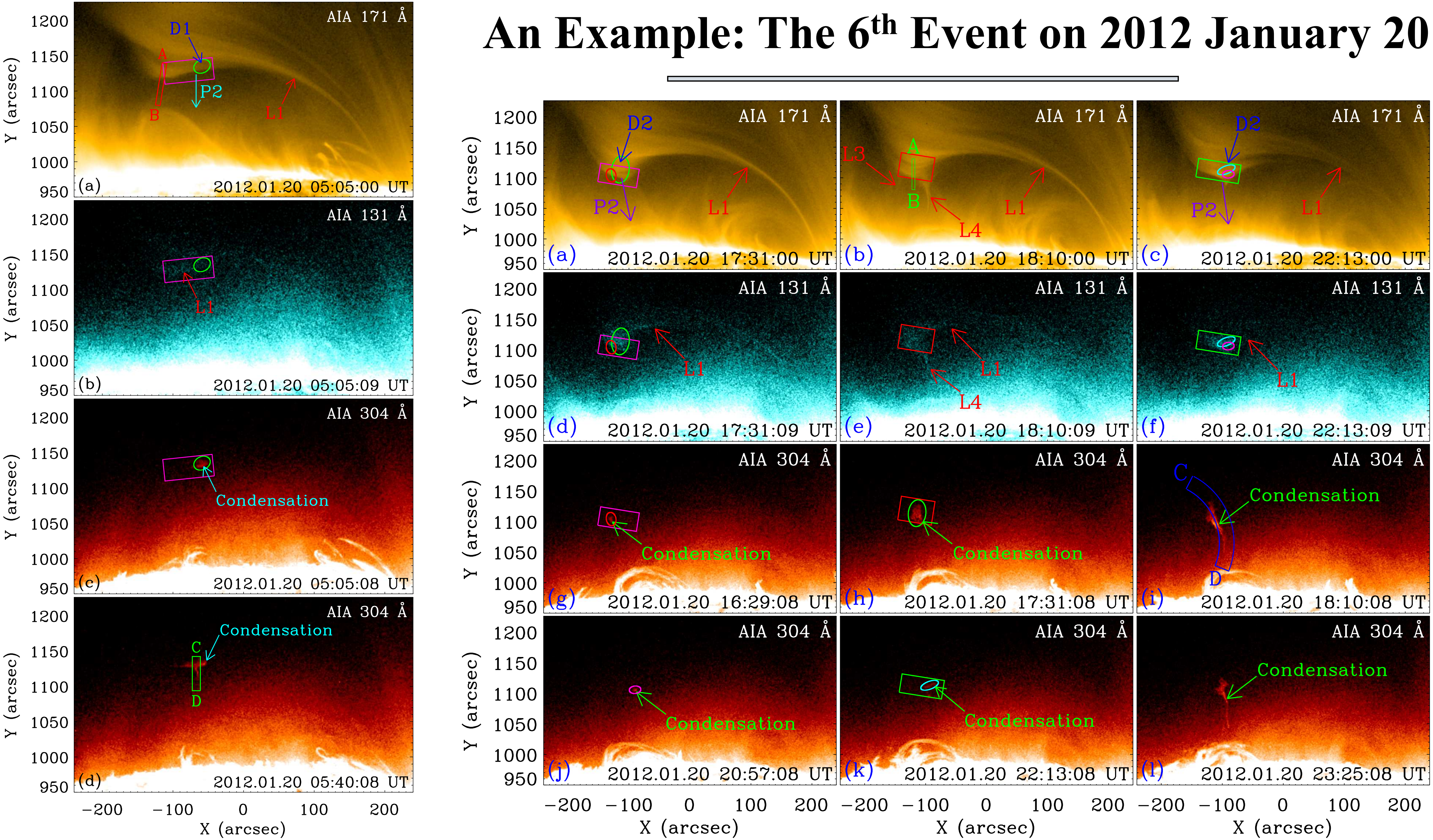

☐ Is **MR-CC** a common phenomenon in other places?

Number	Date	Time (UT)	Position
1	January 1	00:30	N20 E90
2	January 1	18:36	S05 W90
3	January 1	19:10	N30 W90
4	January 1	20:30	S10 W90
5	January 2	00:30	S05 W90
6	January 2	04:05	N30 E90
7	January 2	09:05	N20 E90
8	January 2	14:00	S05 W90
9	January 3	01:30	N20 E90
10	January 3	11:10	N00 E90
11	January 3	13:55	S20 E90
12	January 4	04:20	N20 E90
13	January 4	15:05	S15 E90
14	January 4	18:10	S10 W90
15	January 5	00:30	N10 W90
16	January 5	07:40	S10 W90
17	January 5	09:06	S05 W90
18	January 5	14:10	S05 W90
19	January 6	05:02	N05 W90
20	January 6	08:38	S10 W90
21	January 6	13:40	S05 W90
22*	January 7	02:44	S10 W90
23	January 7	05:25	S20 W90
24	January 7	13:24	S05 W90
25	January 7	17:14	N40 W90
26	January 7	19:59	S10 W90
27	January 8	01:40	S10 W90
28	January 8	11:30	S40 W90
29	January 9	03:35	S40 W90
30	January 9	07:40	S30 W90
31	January 10	05:30	N40 E90
32	January 10	07:26	N40 E90
33	January 10	10:18	S10 E90
34	January 10	14:08	S10 E90
35*	January 10	14:40	N40 E90
36	January 10	22:30	N60 W90
37	January 11	03:20	N60 W90
38*	January 11	12:18	N30 W90
39	January 11	21:33	S15 W90
40	January 12	11:58	N40 W90
41	January 12	17:05	S10 W90
42	January 13	00:43	N40 W90
43	January 13	11:58	S05 W90
44	January 14	00:00	N40 W90
45	January 14	21:47	N49 E90
46	January 15	10:18	N40 E90
47	January 15	22:31	S10 E90
48	January 16	22:30	N10 E90

Table D1 *(continued)*

Number	Date	Time (UT)	Position
49	January 17	11:30	S30 E90
50	January 17	22:02	S50 W90
51	January 18	05:45	S50 W90
52	January 19	13:40	S20 W90
53	January 19	18:10	S10 E90
54	January 20	10:18	S10 E90
55	January 20	10:46	N05 E90
56	January 20	15:48	S20 W90
57	January 21	03:50	N05 E90
58	January 21	05:30	S20 W90
59	January 21	11:30	S10 E90
60	January 22	03:50	N40 E90
61	January 22	16:17	S10 E90
62	January 22	15:05	S20 W90
63	January 23	11:26	S20 W90
64	January 23	12:52	N60 W90
65	January 23	17:25	N20 W90
66	January 24	12:56	S10 W90
67	January 24	17:44	N05 E90
68	January 25	21:47	N80 E90
69	January 26	06:43	N20 W90
70	January 27	15:46	S10 E90
71	January 28	23:14	N40 E90
72	January 28	23:44	N15 W90
73	January 29	05:14	N45 E90
74	January 29	08:14	S20 E90
75	January 29	08:44	N10 W90
76	January 30	01:20	S55 E90
77	January 30	19:29	N02 E90
78	January 31	02:00	N20 W90
79	January 31	02:45	N60 E90

* The events displayed in Figure D1.

NOTE—The third column shows the time when the loops L1 and coronal condensations are simultaneously observed in AIA 171 Å and 304 Å images, respectively.

79 Similar Events in 2012 January

- We roughly check the AIA images in January 2012 above the solar limb using 15 minute time cadence.
- 79 similar events are detected in the month alone at different positions and times.
- Three cases among them are displayed, see lower figure.

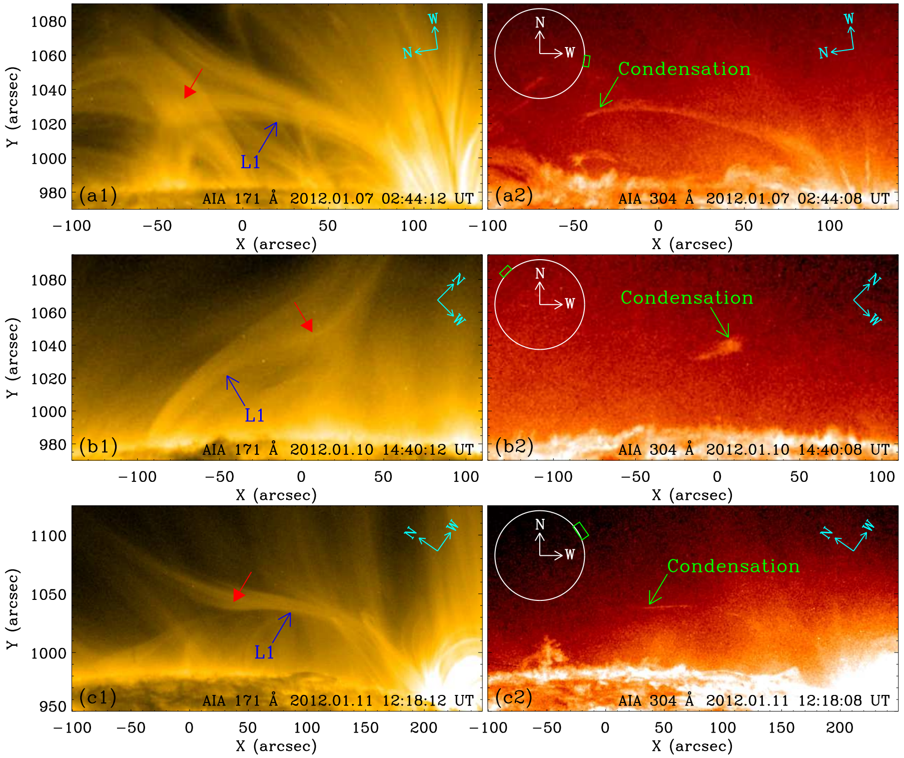

- This kind of **MR** is a common phenomenon in the corona.
- **CC** of coronal plasma always takes place during this kind of **MR**.

2.4 Chromospheric CR Originating from MR-CC

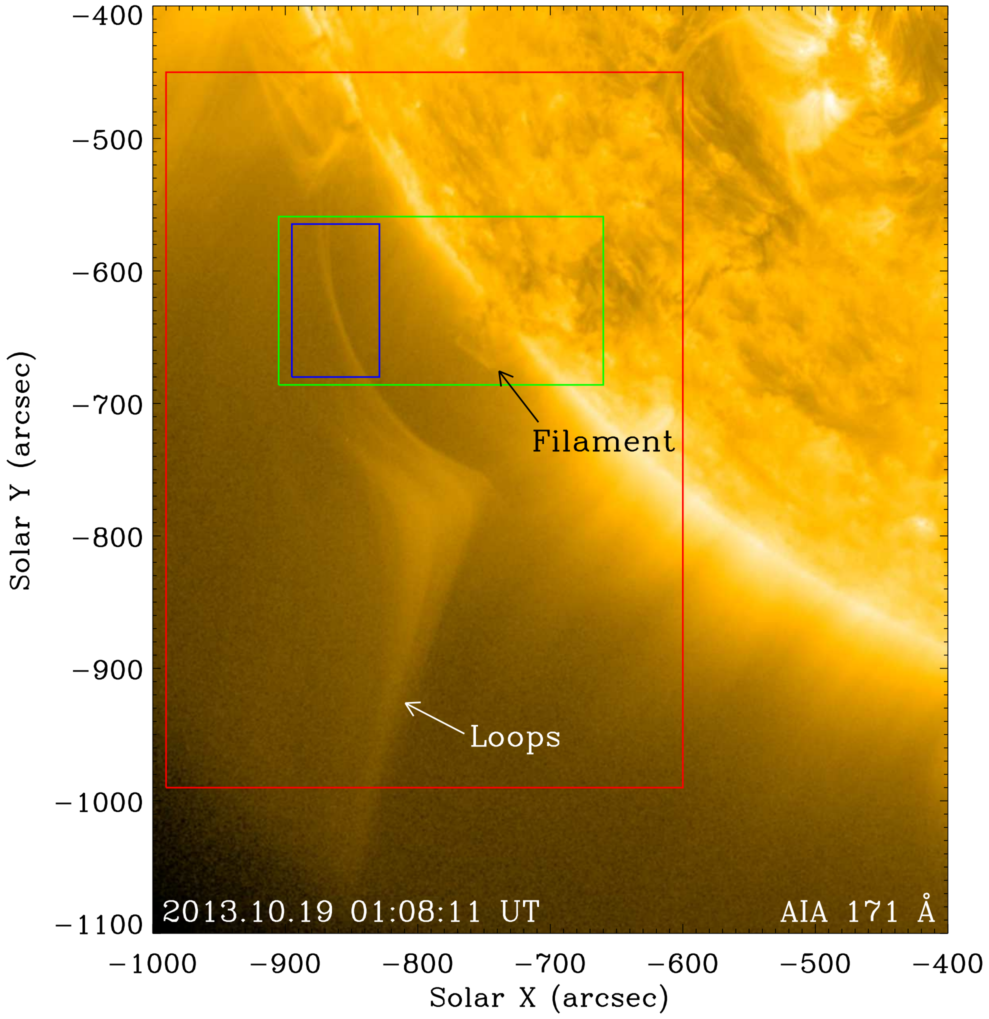

General information of **CR** event (green rectangle shows the FOV of IRIS SJIs) (Li+, 2020, ApJ, 905, 26)

IRIS CR Event

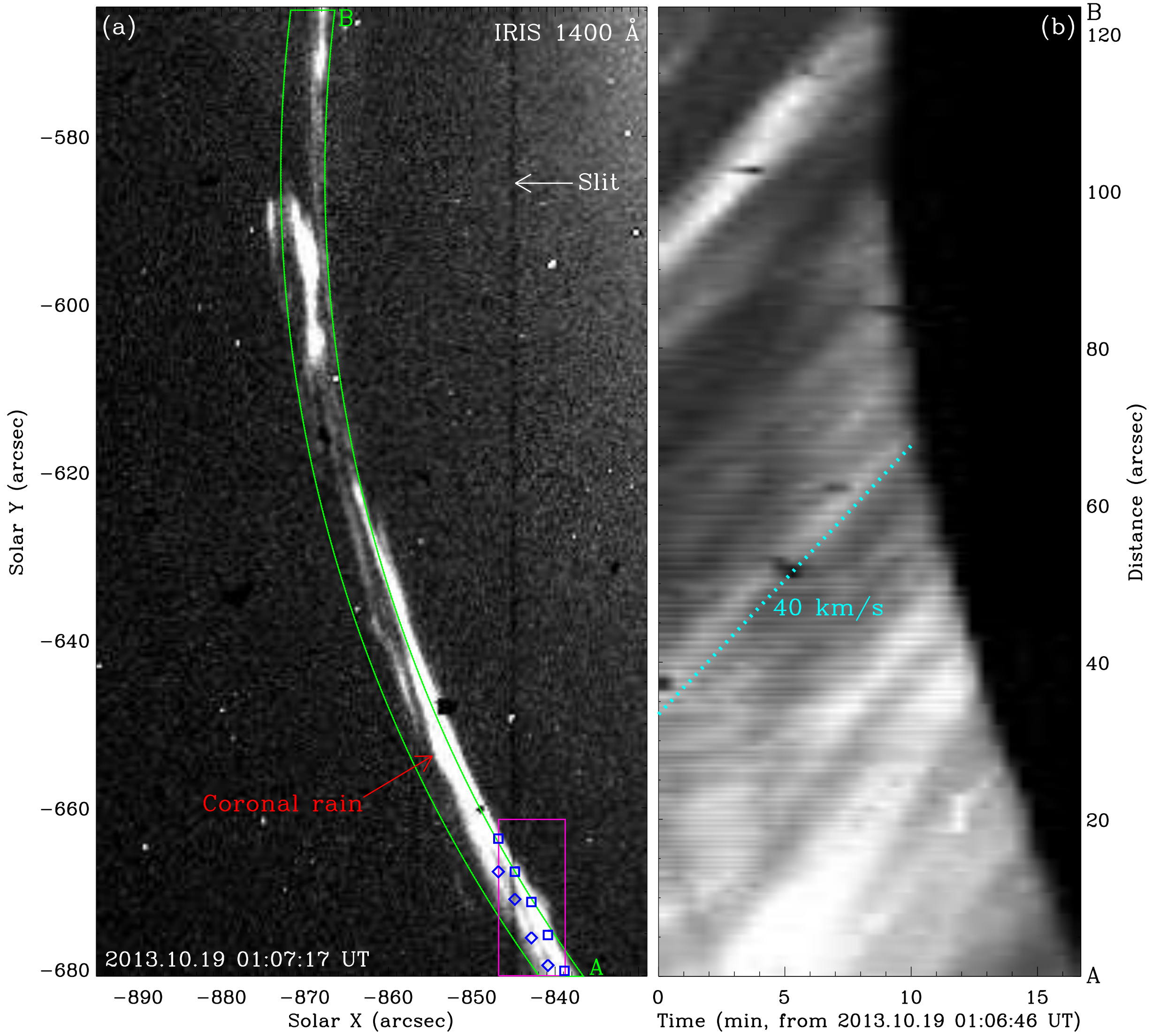

The animation (left) and time slice (right) show the **CR**.

Spectral Information of the IRIS CR

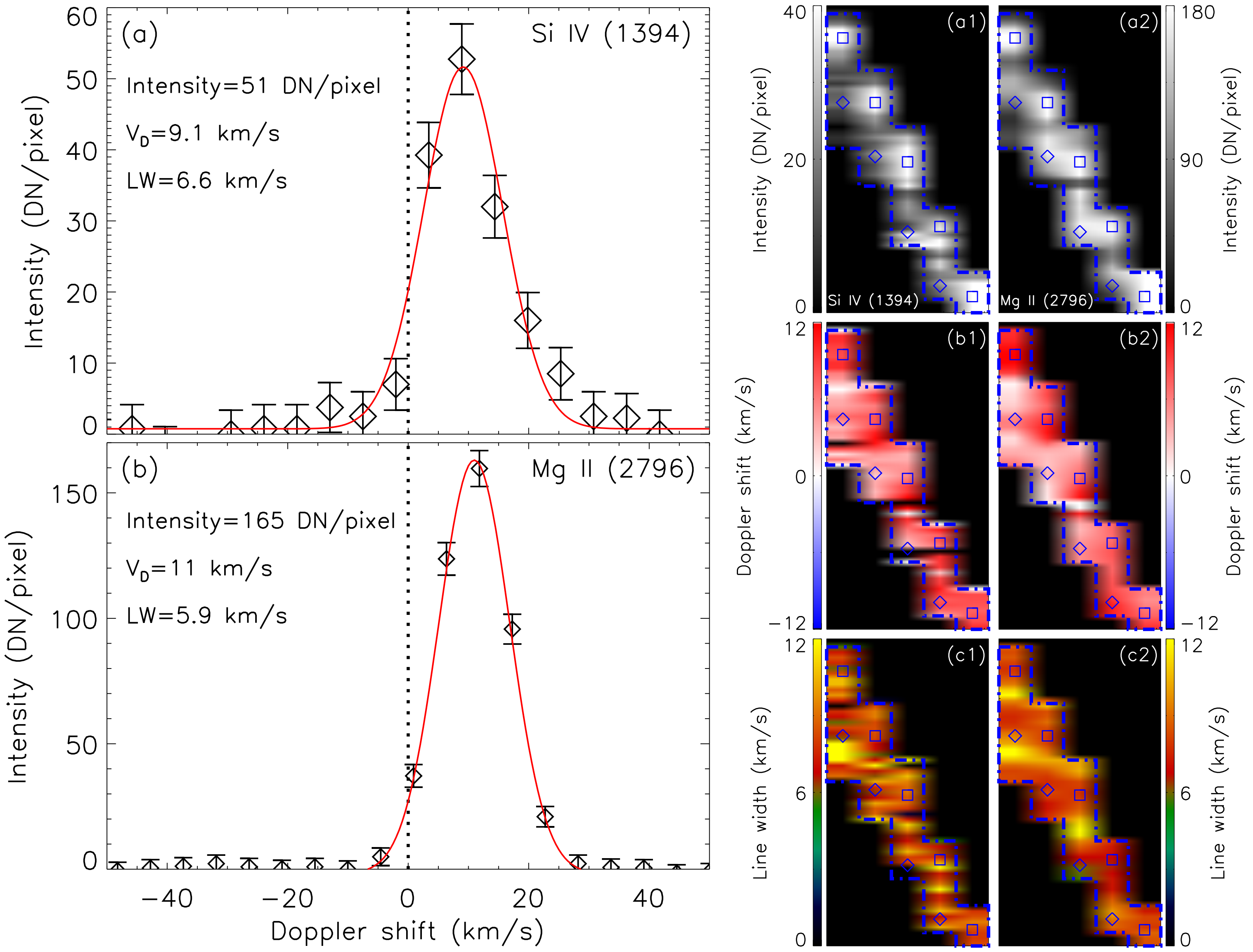

Coronal plasma cools further down to ~0.01 MK (Mg II k at 2796 Å).

MR-CC Observed by AIA

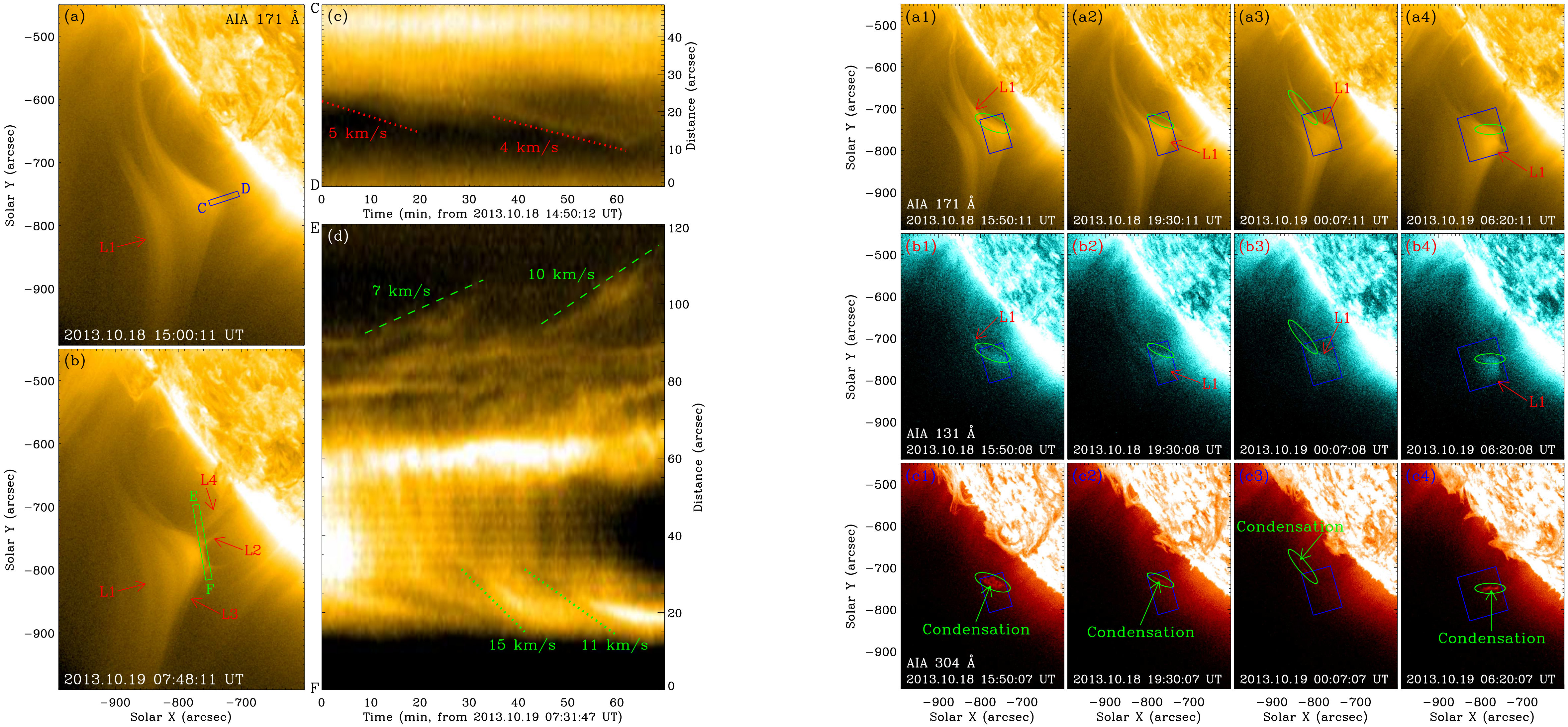

MR (left) and **CC** (right)

Spatial-temporal Relation between MR-CC and IRIS CR

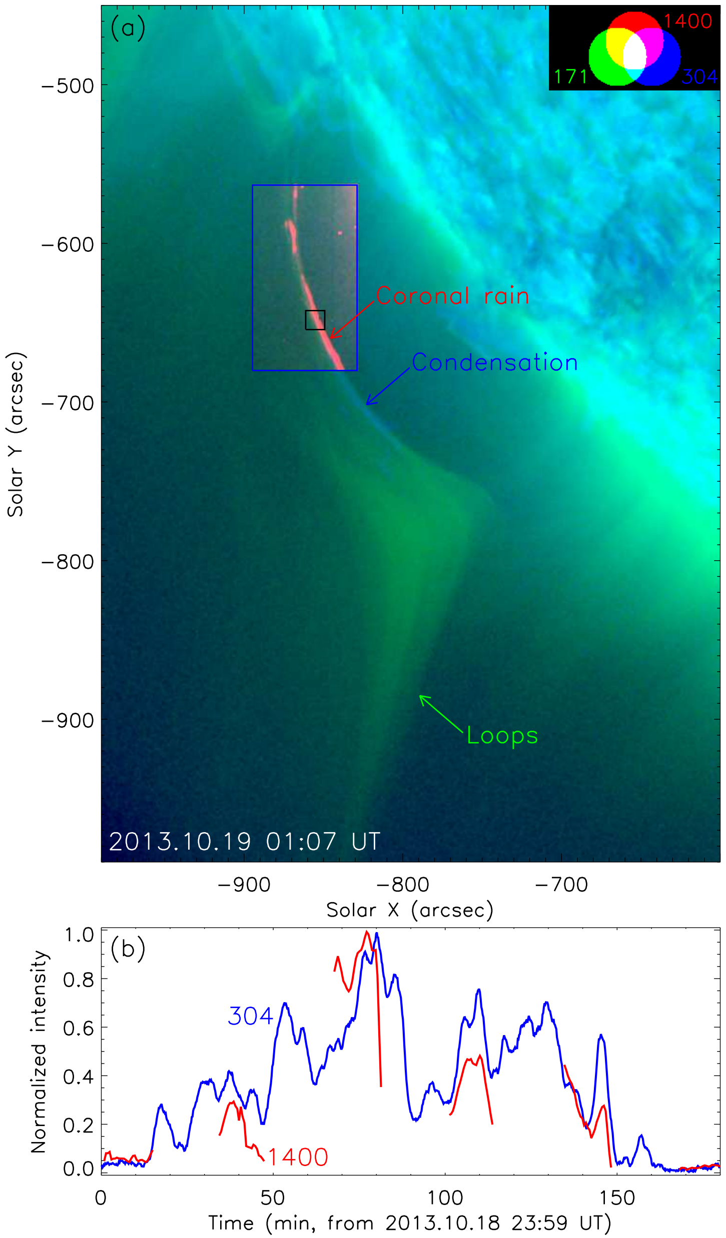

- IRIS **CR** originates from **MR-CC**.
- The new and alternative formation mechanism for **CR** by interchange **MR** is suggested to explain some **CR** events in transition region and chromospheric lines.

2.5 On-disk MR-CC Events

- 2010 September to 2011 September, when the viewing directions of STEREO A and B are mostly perpendicular to that of SDO.
- Evolution of loops and plasma out of the western (eastern) limb in the FOV of STEREO A (B) EUV images.
- **MR-CC** events from 2011 July 14 to 15 are chosen. (Li+, 2021a, ApJ, 910, 82)

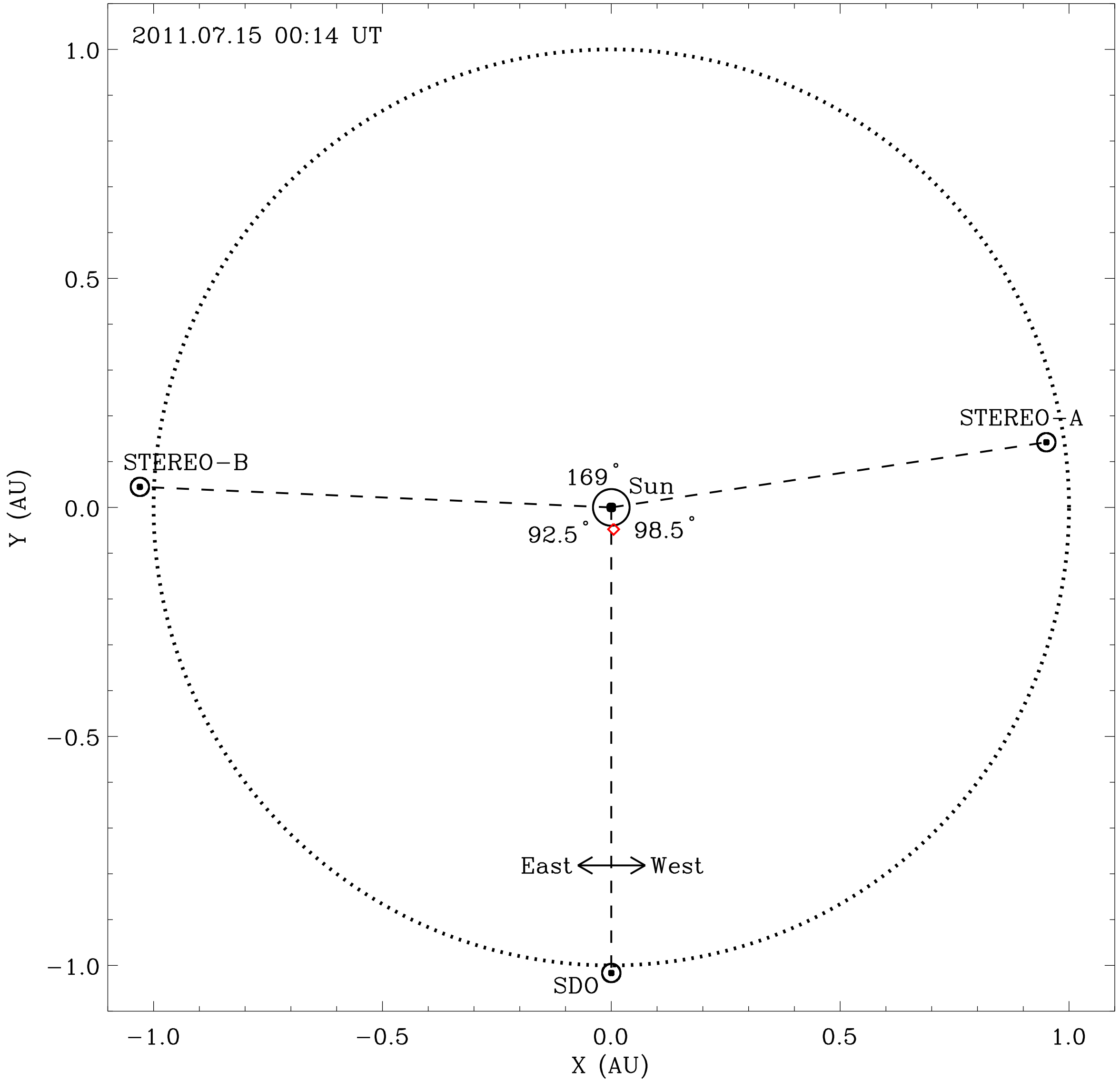

General Information of Structure System

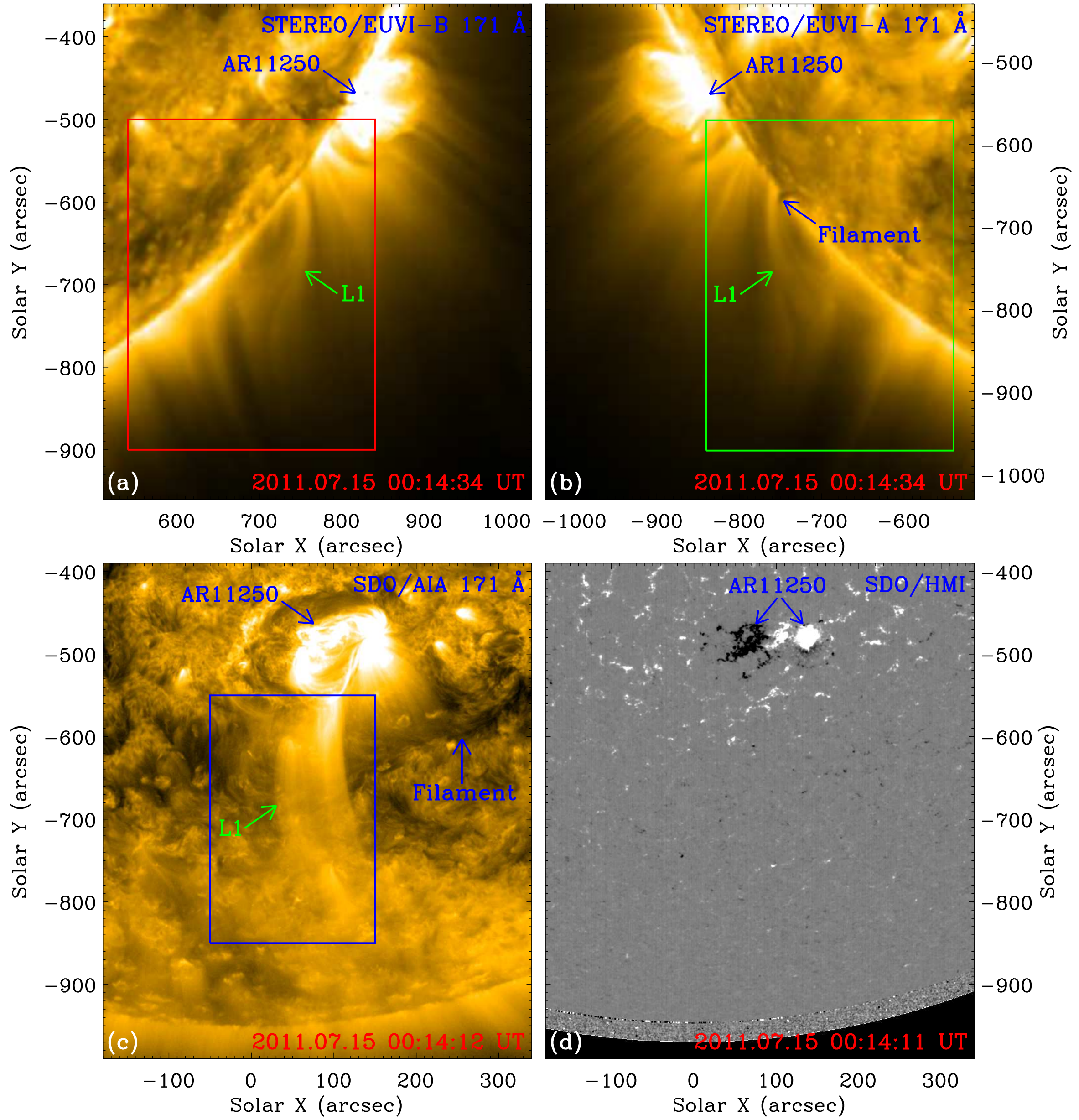

MR-CC Observed by STEREO (Left) and SDO (Right)

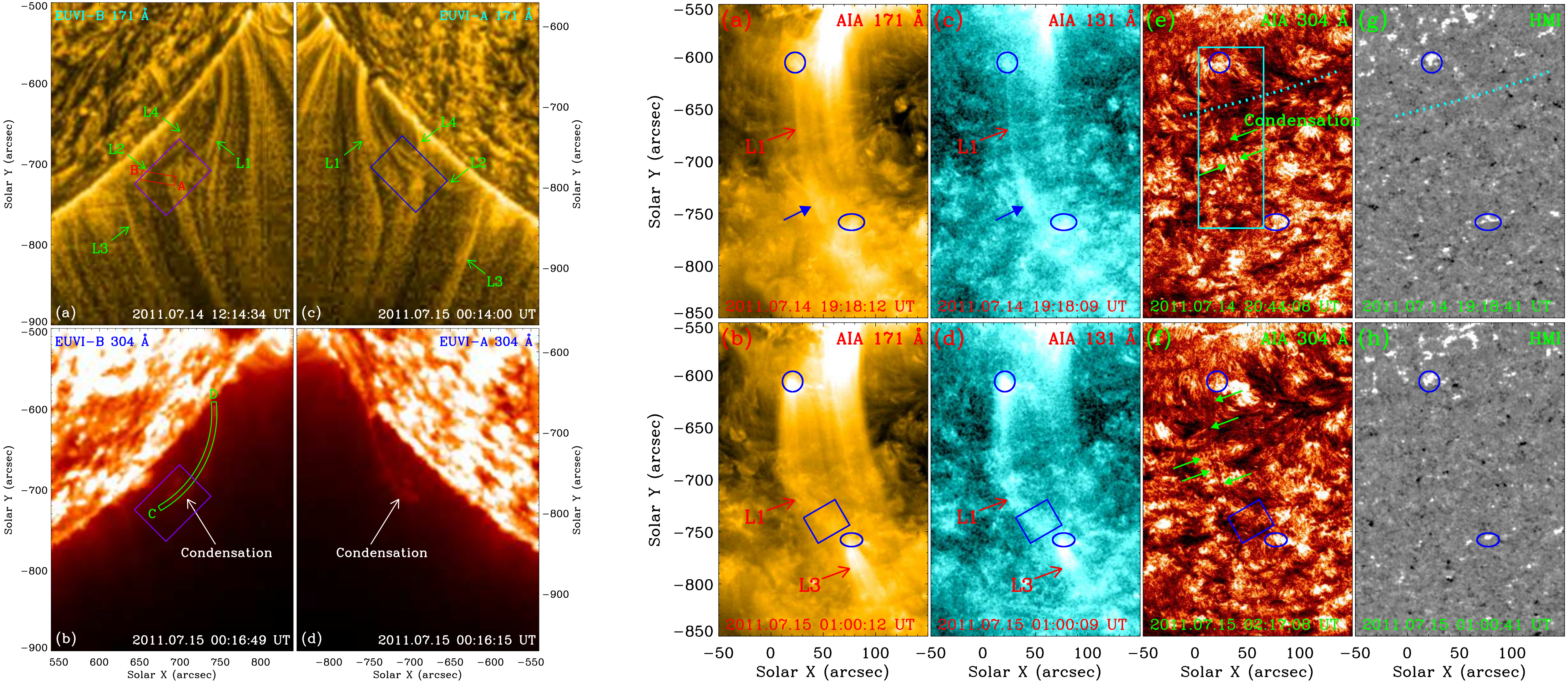

- On-disk **MR-CC** events are identified. Bright emission appears in AIA 171 and 131 Å images, **MR-CC** shows dark absorption feature on the disk.

2.6 Revisiting The Formation Mechanism of CR from Previous Studies

Table 1: General information of the coronal rain events from previous studies.

No.	References	Date	Source region	Coordinate	Position	Observations	Original FM	SDO	Revised FM
1	Li et al. (2021a)	2011.07.14 -07.15	Near AR 11250	S40 W02	On-disk Off-limb	SDO; STEREO	FM-II-2	Yes	-
2	Kumar et al. (2021)	2015.04.20	Plage	N07 E90	Off-limb	SDO	FM-II-1; FM-II-2	Yes	-
		2015.04.21	AR 12333	N20 E90					
		2015.01.09	AR 12261	S11 E90					
3	Li et al. (2020)	2013.10.18 -10.19	Quiet Sun	S45 E90	Off-limb	SDO; IRIS	FM-II-2	Yes	-
4	Ishikawa et al. (2020)	2014.04.24	AR 12042	N22 W32	On-disk	SDO; IRIS	FM-II-1	Yes	-
5	Froment et al. (2020)	2017.08.28 -08.30	AR 12674	N10 E90	Off-limb	SDO; SST	FM-II-1	Yes	FM-II-1
6	Li et al. (2019)	2012.01.16 -01.20	Quiet Sun	N50 W90	Off-limb	SDO; STEREO	FM-II-2	Yes	-
7	Kohutova et al. (2019)	2015.12.09	AR 12468	S13 E90	Off-limb	SDO; IRIS	FM-II-1	Yes	FM-II-1
8	Mason et al. (2019)	2015.04.16	Sharp 5437	N00 W90	Off-limb	SDO	FM-II-1; FM-II-2	Yes	-
		2015.05.04	AR 12333	N22 W90					
		2016.02.27	AR 12488	N04 W90					
9	Vashalomidze et al. (2019)	2011.10.06 -10.07	Near AR 11312	N40 E90	Off-limb	SDO	FM-II-1	Yes	FM-II-1
10	Li et al. (2018a,b)	2012.01.19	Quiet Sun	N50 W90	Off-limb	SDO	FM-II-2	Yes	-
11	Schad (2017, 2018)	2015.12.09	AR 12468	S00 E90	Off-limb	SDO; IRIS; DST	FM-II-1	Yes	FM-II-1; FM-II-2
12	Auchère et al. (2018)	2012.07.23 -07.25	AR 11532	S00 E90	Off-limb	SDO	FM-II-1	Yes	FM-II-1; FM-II-2
13	Lacatus et al. (2017)	2015.03.11	AR 12297	S10 E20	On-disk	SDO; IRIS	FM-I	Yes	-
14	Verwichte & Kohutova (2017)	2014.08.27	AR 12141	N20 W90	Off-limb	SDO; IRIS; Hinode	FM-II-1	Yes	FM-II-1
15	Verwichte et al. (2017)	2012.04.16	AR 11461	N17 W90	Off-limb	Hinode	FM-II-1	Yes	FM-II-1
16	Scullion et al. (2016, 2014)	2012.07.02	AR 11515	S17 E14	On-disk	SDO; SST	FM-II-1	Yes	-
		2012.07.01	AR 11515	S20 E23	On-disk	SDO; SST	FM-I	Yes	-
		2011.09.24	AR 11302	N10 E60					
17	Kohutova & Verwichte (2016)	2014.08.25	Near AR12151	S13 E90	Off-limb	SDO; IRIS; Hinode	FM-II-1	Yes	FM-II-1
18	Reeves et al. (2015)	2014.05.01	AR 12044	S20 W90	Off-limb	SDO; IRIS	-	Yes	FM-II-2
19	Antolin et al. (2015)	2010.06.26	AR 11084	S20 E72	Off-limb	SST; SDO	FM-II-1	Yes	FM-II-1
		2013.11.29	AR 11903	S15 W90	Off-limb	SDO; IRIS; Hinode			
20	Vashalomidze et al. (2015)	2012.02.22	AR 11420	N10 E90	Off-limb	SDO; STEREO	FM-II-1	Yes	FM-II-2
21	Liu et al. (2015)	2014.05.09	AR 12051	S17 W90	Off-limb	SDO; IRIS	FM-II-1	Yes	FM-II-1
22	Ahn et al. (2014)	2011.09.29	AR 11305	N12 E14	On-disk	SDO; NST; STEREO	FM-II-1	Yes	-
23	Liu et al. (2012)	2010.11.26	AR 11126	S32 W90	Off-limb	SDO	-	Yes	FM-II-2

Table 1: (Continued)

No.	Reference	Date	Source region	Coordinate	Position	Observations	Original FM	SDO	Revised FM
24	Antolin et al. (2012)	2008.06.10	AR 10998	S07 E63	On-disk	SST	FM-II-1	No	-
		2008.06.11	AR 10998	S09 E46					
		2010.06.27	AR 11084	S19 E65	On-disk	SST	FM-II-1	Yes	
		2010.06.28	AR 11084	S19 E45					
		2010.07.06	AR 11084	S19 W60					
25	Antolin & Rouppe van der Voort (2012)	2009.05.10	AR 11017	N18 E90	Off-limb	SST; Hinode	FM-II-1	No	-
26	Kamio et al. (2011)	2010.10.31	AR 11117	N20 W90	Off-limb	SDO	FM-II-1	Yes	FM-II-2
		2010.11.05	AR 11120	N38 W09	On-disk	SDO; Hinode	FM-II-1	Yes	-
27	Antolin et al. (2010); Antolin & Verwichte (2011)	2006.11.09	AR 10921	S06 W80	Off-limb	Hinode	FM-II-1	No	-
28	Zhang & Li (2009)	2007.05.10	Quiet Sun	S02 E90	Off-limb	STEREO; Hinode	FM-II-1	No	-
29	O'Shea et al. (2007)	2003.03.21	AR 10314	S13 W90	Off-limb	TRACE; SOHO	FM-II-1	No	-
30	De Groof et al. (2004, 2005); Müller et al. (2005)	2001.07.11	AR 9538	N17 E90	Off-limb	SOHO; BBSO	FM-II-1	No	-
31	Brosius (2003)	2001.06.15	AR 9502	S26 E48	On-disk	SOHO	FM-I	No	-
32	Schrijver (2001)	2000.05.26	AR 9004	N11 W83	Off-limb	TRACE	FM-II-1	No	-
		1999.05.29	AR 8531	N17 E90					

- 38 refereed papers on **CR** are selected.
- 4 FM-I; 28 FM-II-1; 7 FM-II-2. (Li+, 2021b, RAA, 21, 255)

Results

- The **CR** events occurred before the launch of the SDO are not revisited.
- The on-disk **CR** events are not revisited.
- The quiescent **CR** events that have been identified to occur along open structures and the flare-driven **CR** events are not revisited.

- At last, 15 **CR** events, mostly suggested to form along non-flaring AR closed loops due to thermal nonequilibrium, are selected to recheck their formation mechanism.
- After investigating the evolution of these 15 **CR** events and their magnetic fields and context coronal structures, we find that 6 of 15 events could be totally or partially explained by the formation mechanism for quiescent **CR** along open structures facilitated by interchange **MR**.

An Example: MR-CC event on 2014 May 1

In this active region, Reeves et al. (2015) studied the filament eruption and the **MR** between filament and open structures.

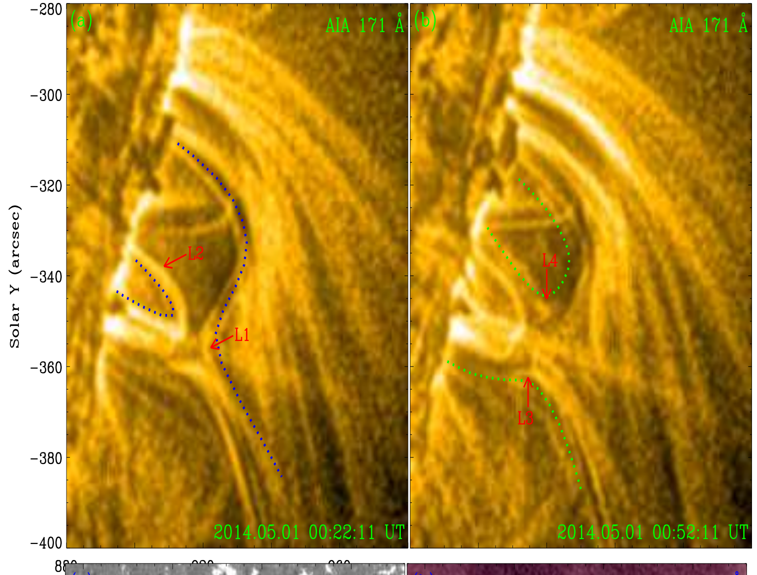

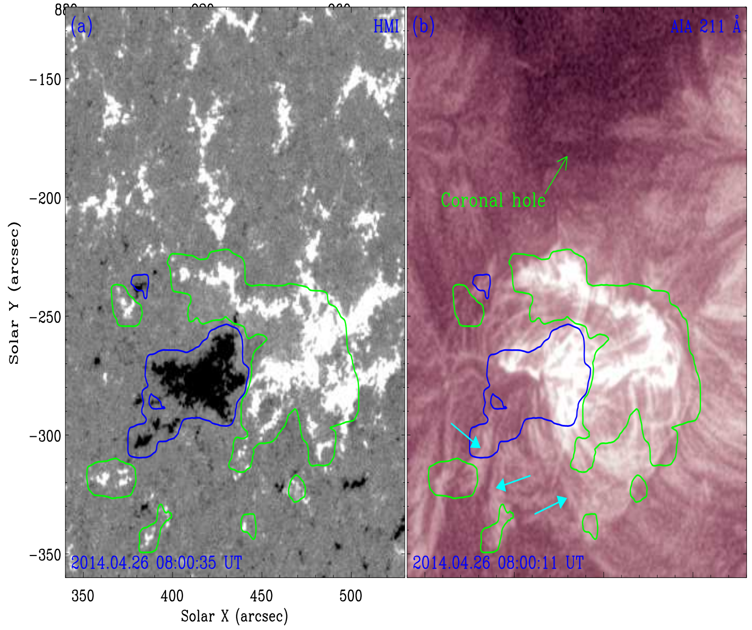

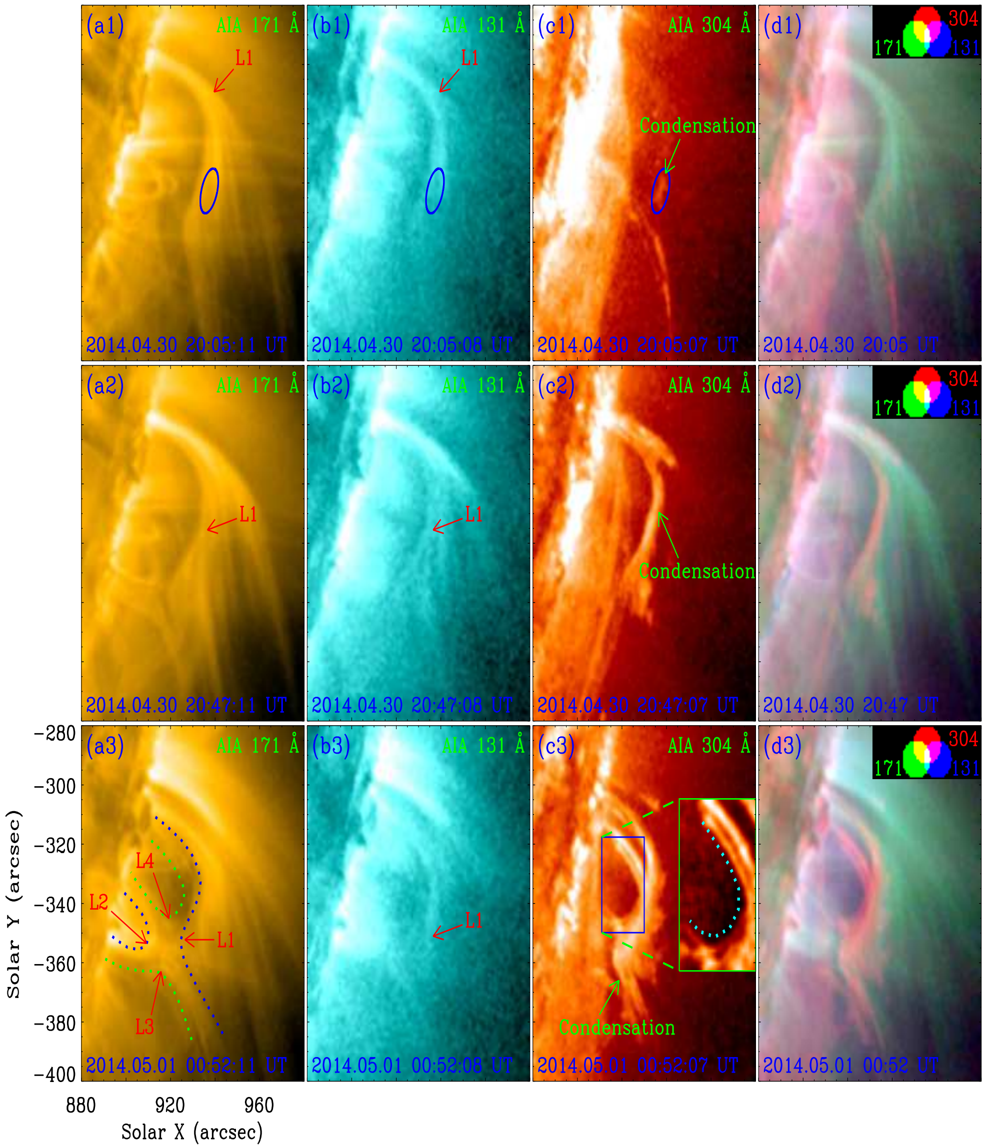

MR (upper-left), **CC** (right), and magnetic fields (lower-left) in a fan-spine active region (Mason+ 2019)

2.7 MR-CC as The Source of Supersonic Downflows Above A Sunspot

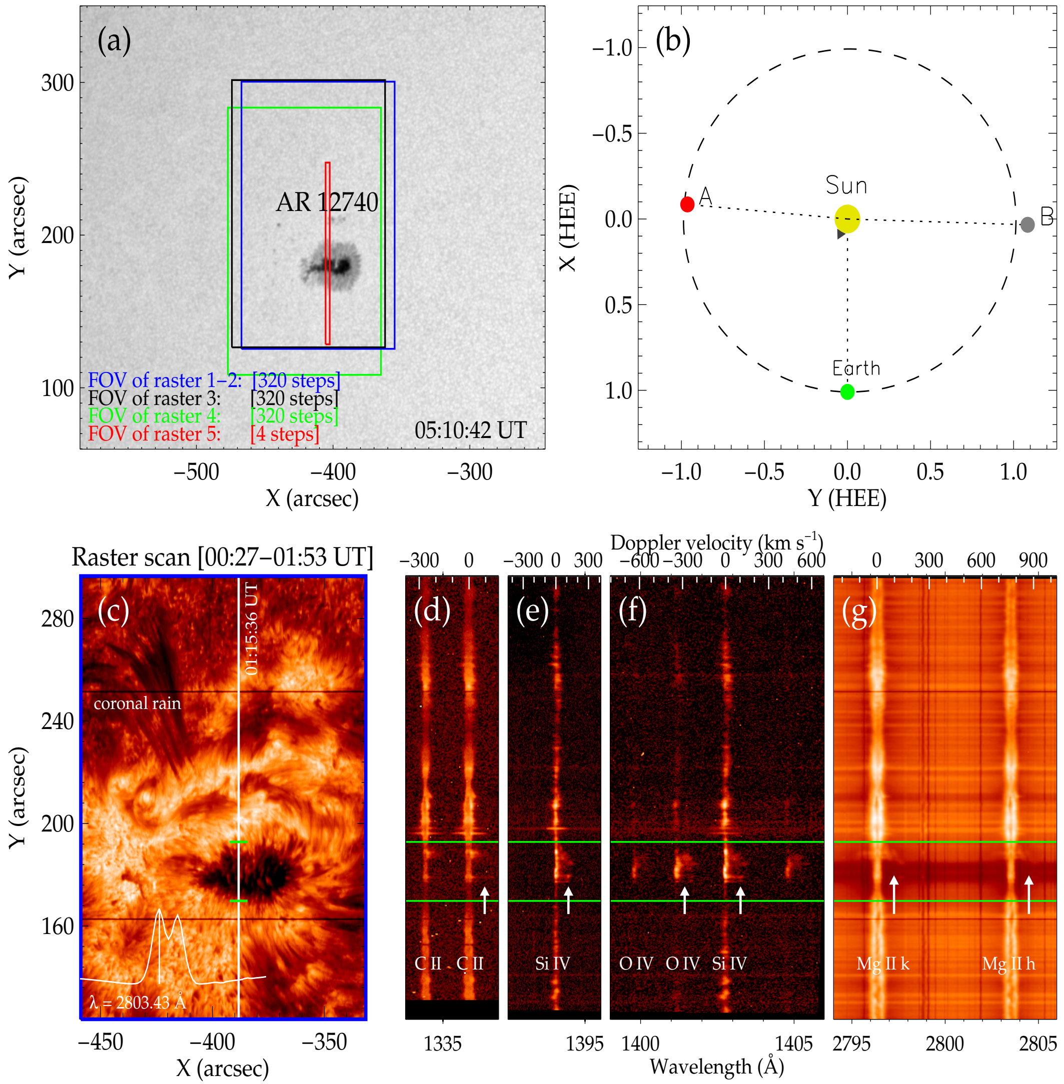

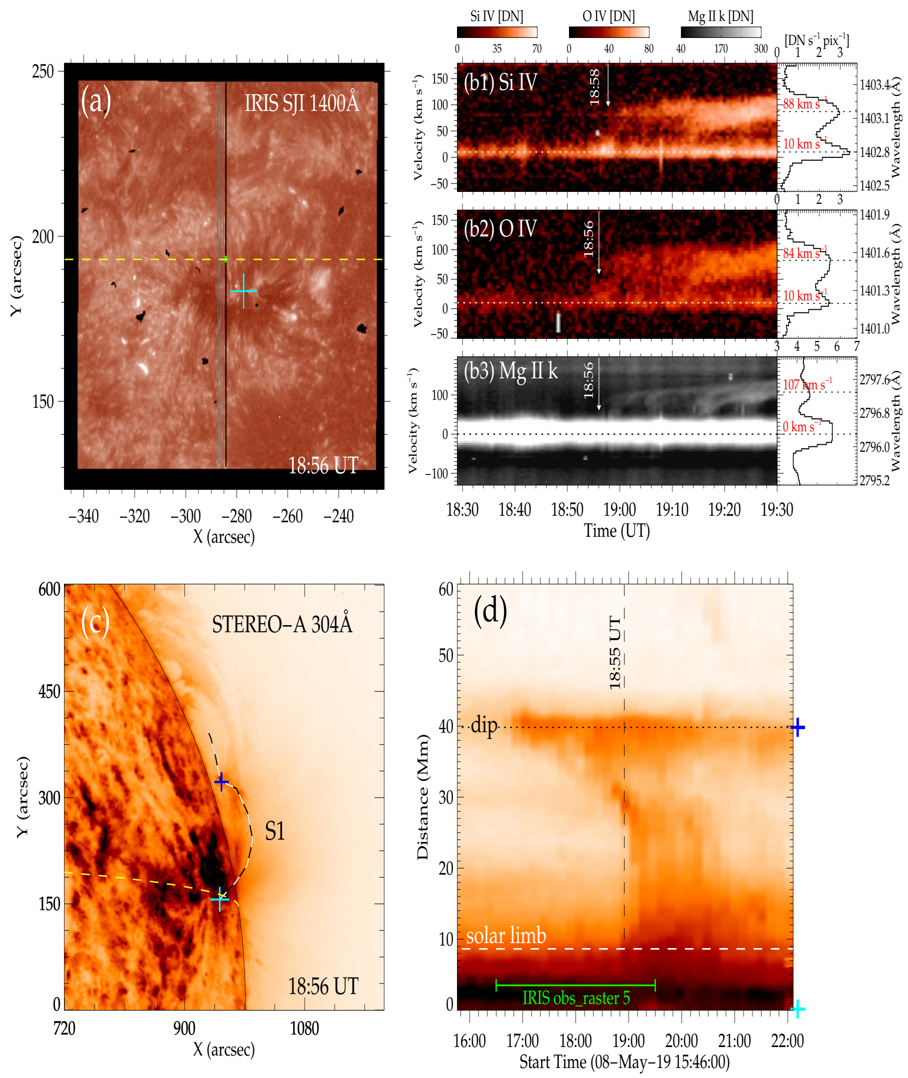

Supersonic downflows observed by IRIS (Chen+ 2022, A&A, 659, A107)

MR-CC Observed by STEREO (Left) and SDO (Right)

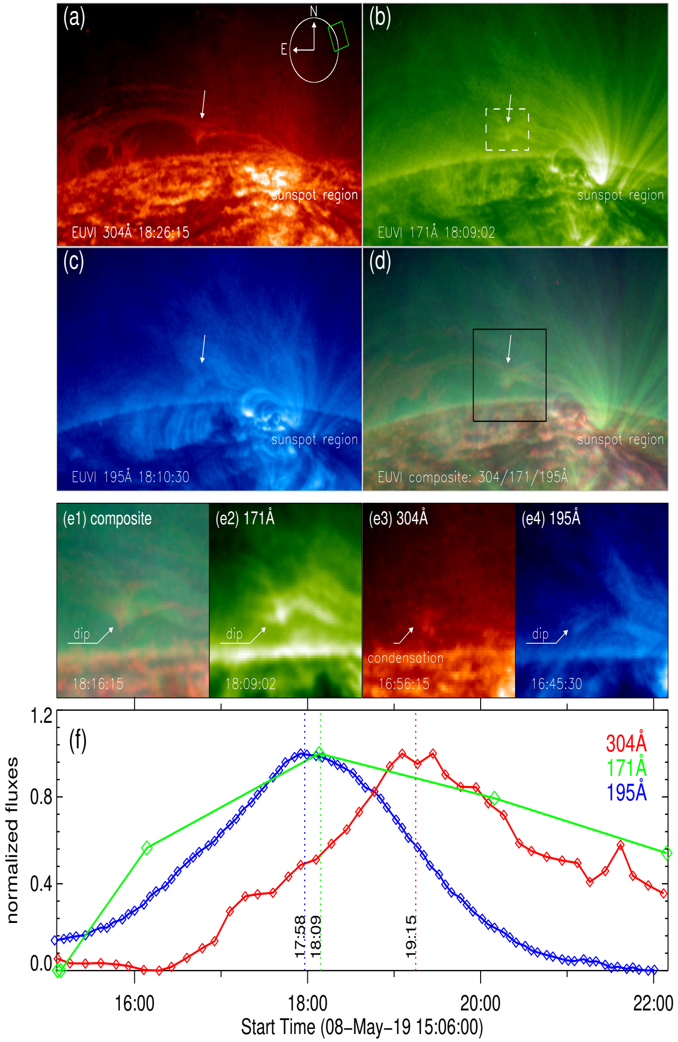

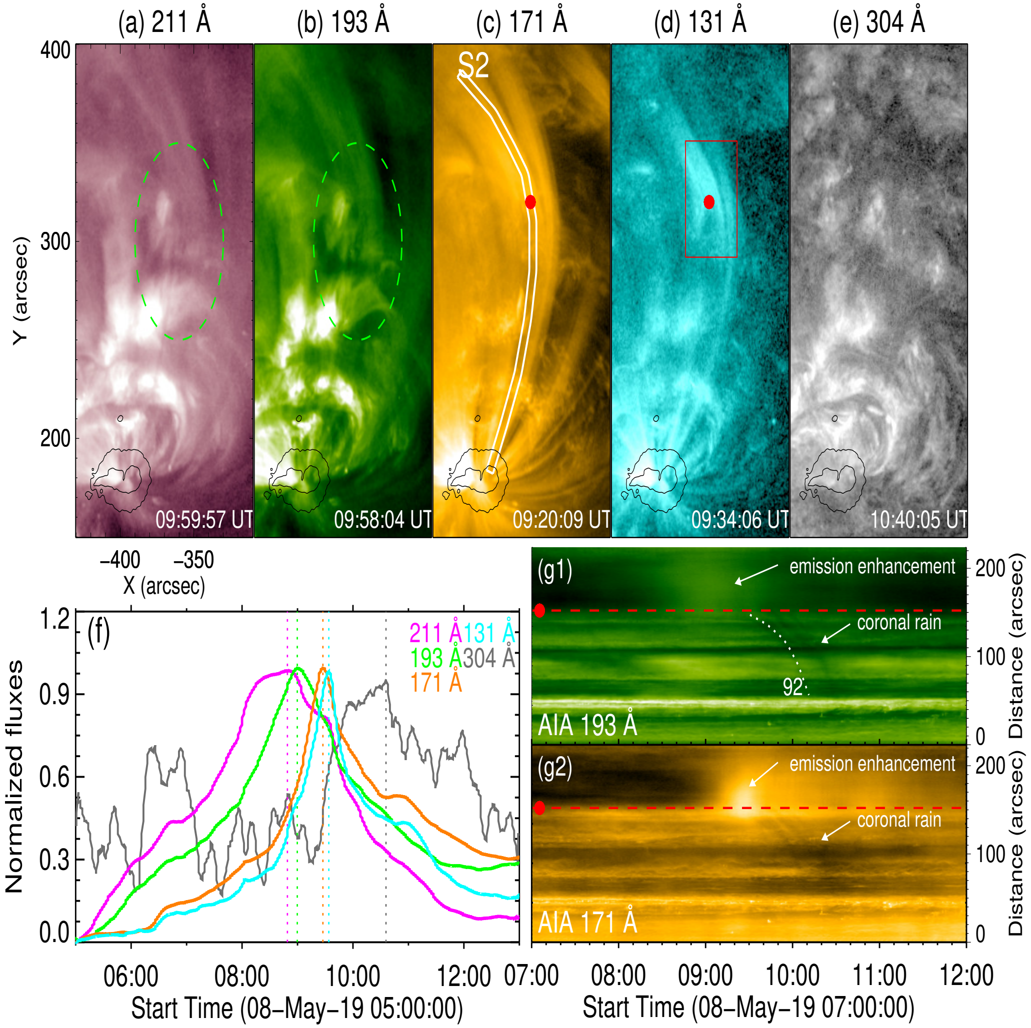

- Spatial and temporal relationship between the **CR** by **MR-CC** and the supersonic downflows shows that the supersonic downflows originate from the **MR-CC**.

2.8 Formation of a (Channel) Filament by MR and CC

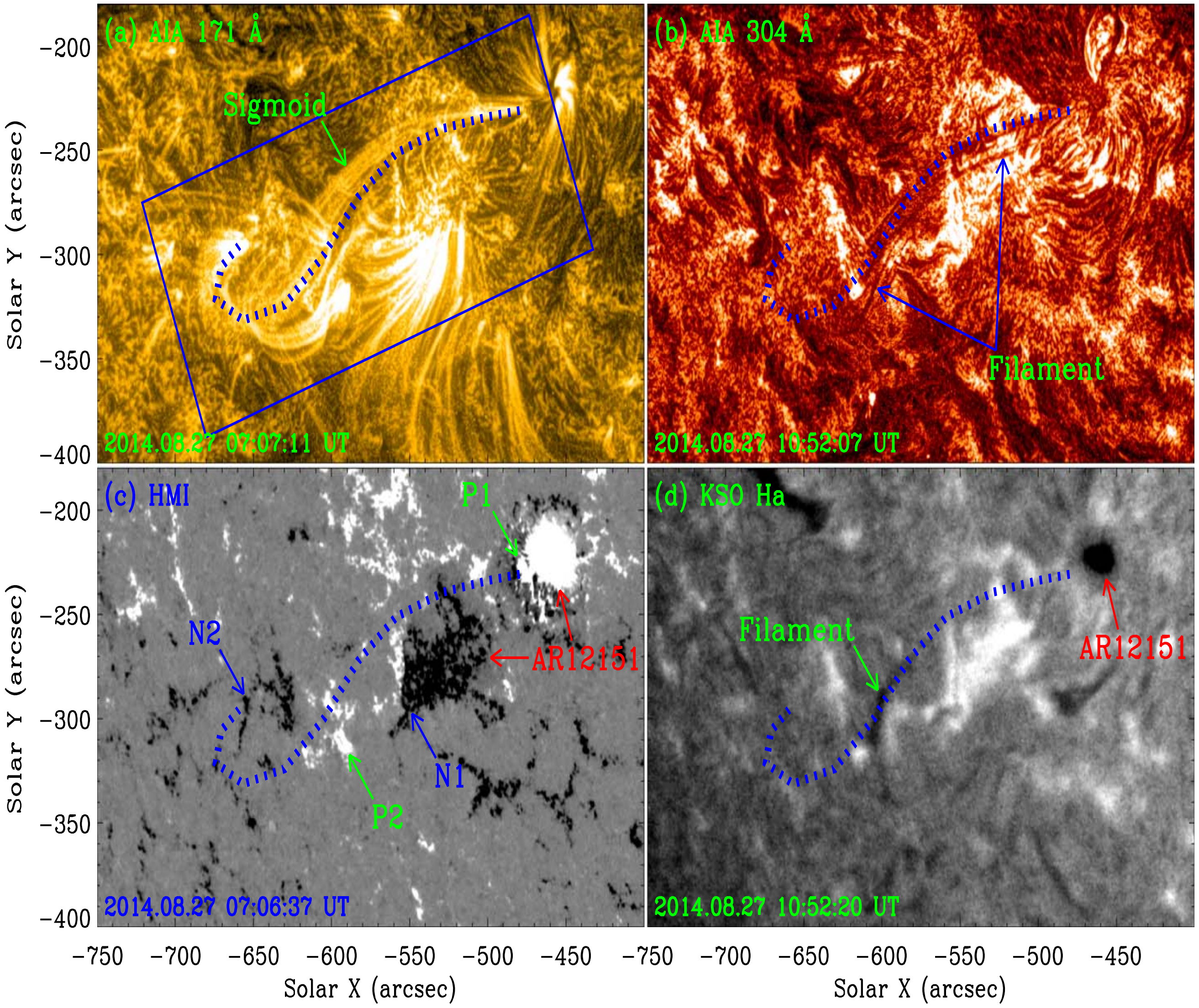

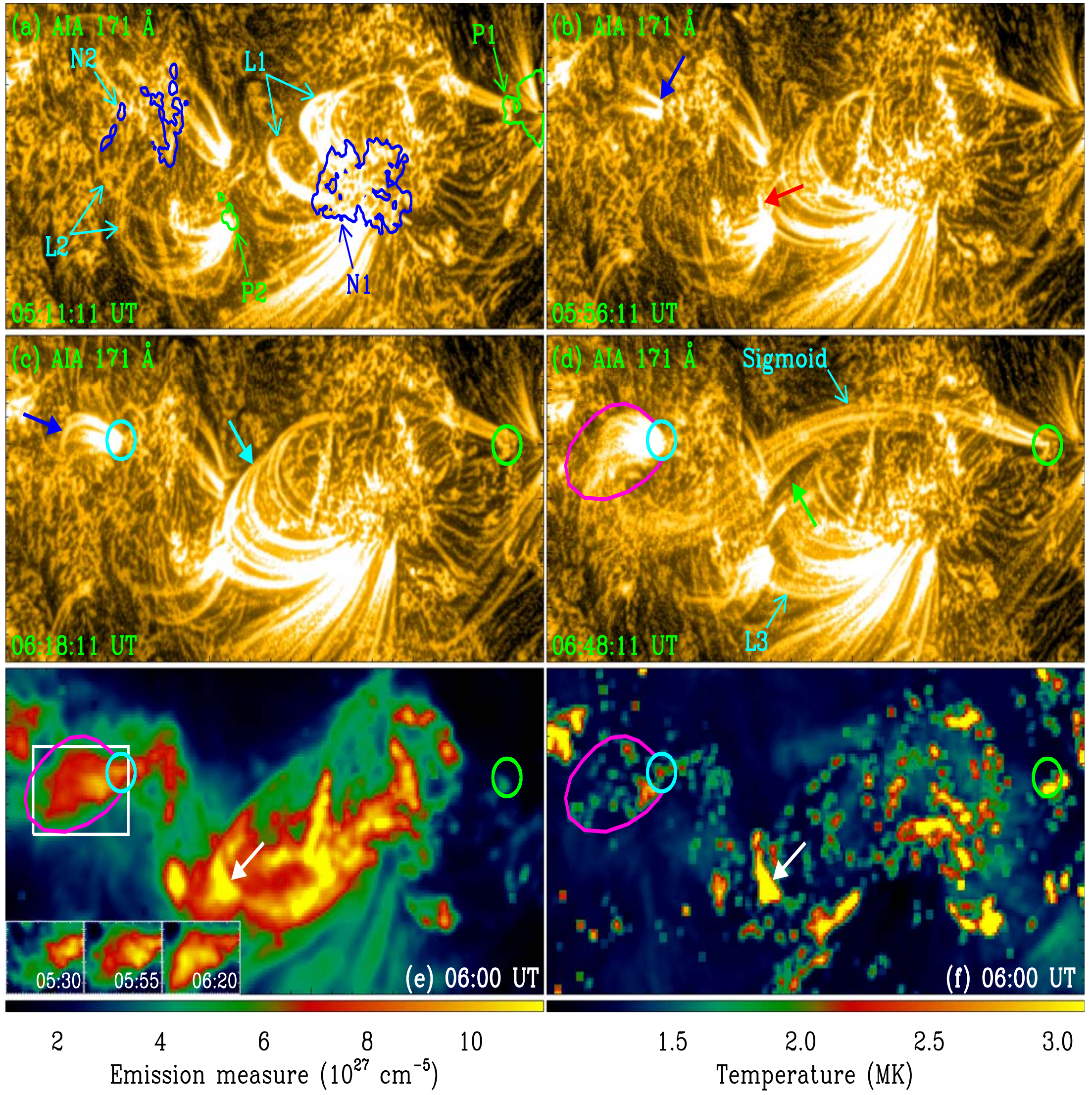

General information (Li+ 2021c, ApJL, 919, L21)

Tether-cutting **MR** forming a sigmoid & Chromospheric evaporation

Filament Formation by CC

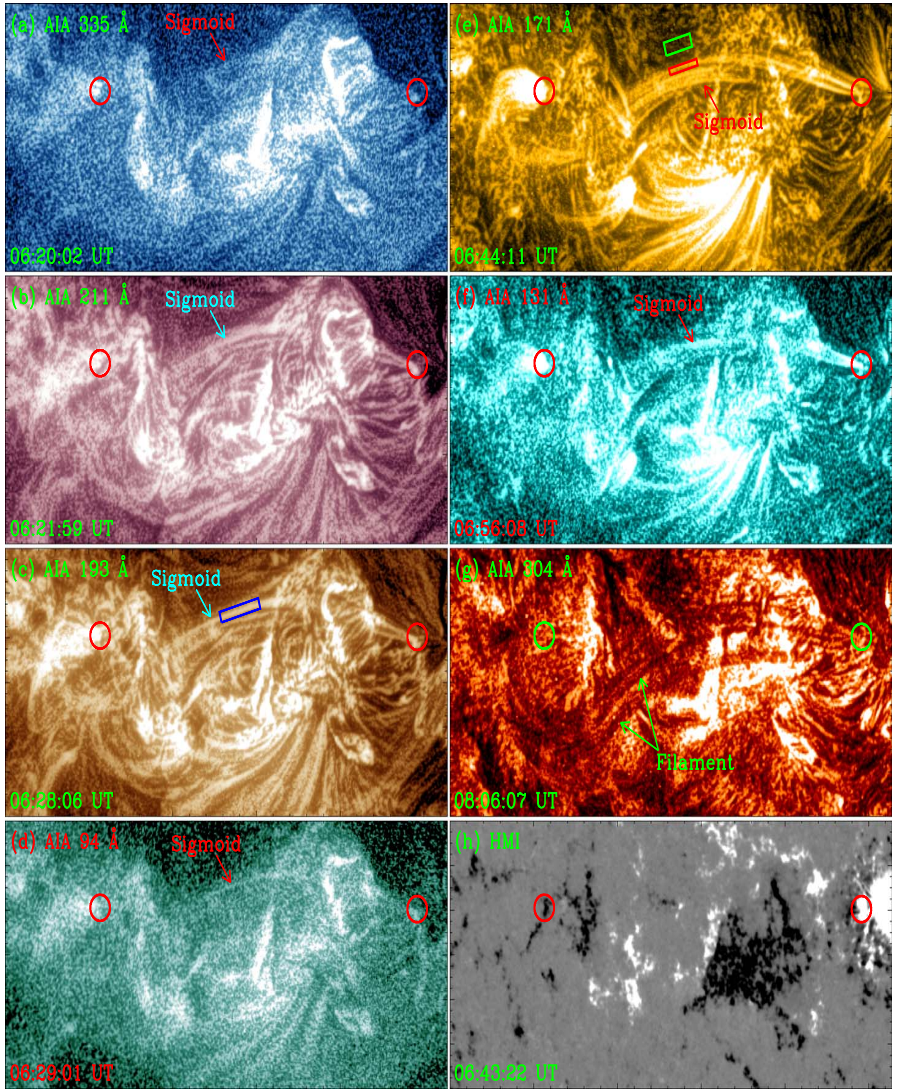

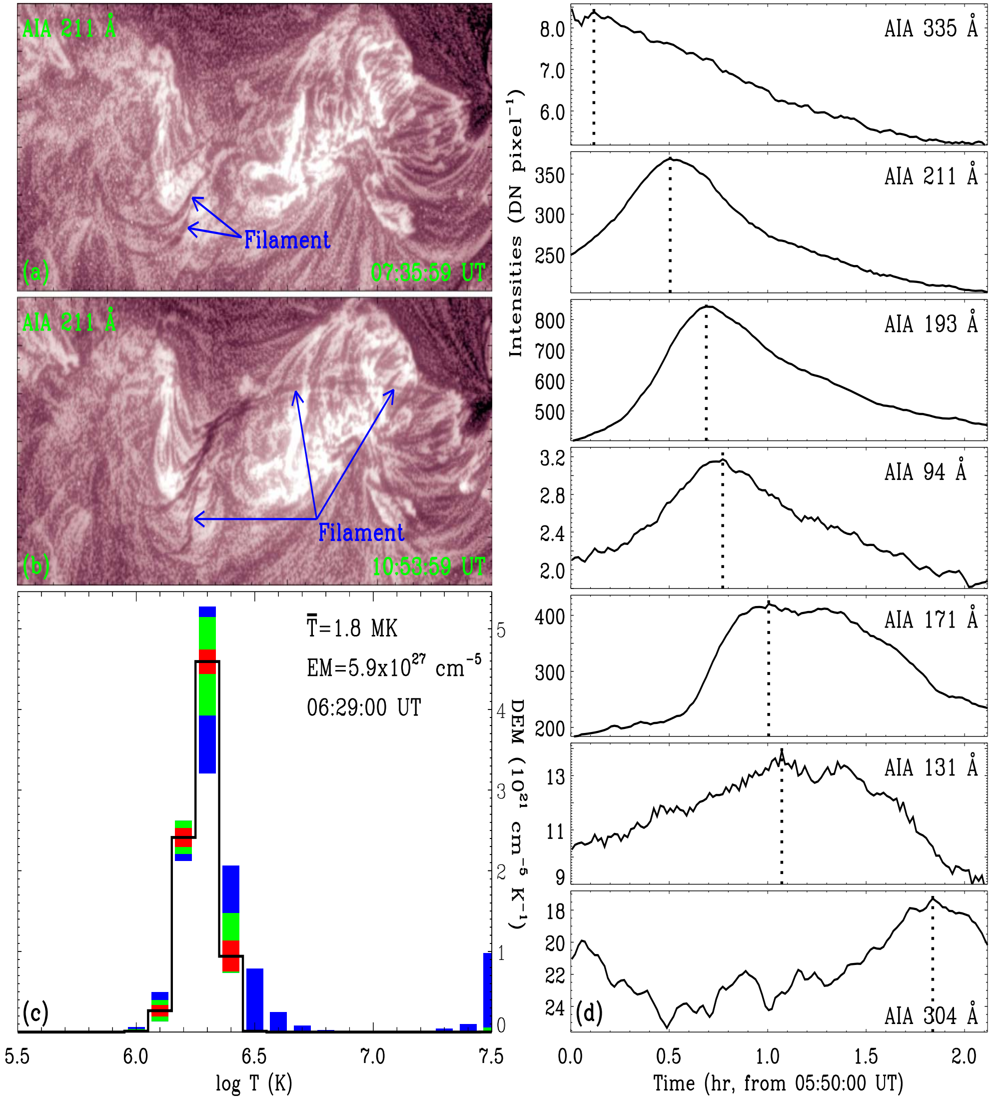

Cooling and **CC** of the Sigmoid

Sigmoid and the subsequent filament formed by **MR** and **CC**

3. Summary

- A new and alternative formation mechanism for **CR** facilitated by **MR** between open and closed magnetic structures is proposed (Li+ 2018a, ApJL, 864, L4).
- Magnetic energy is mainly converted to wave energy by **MR** (Li+ 2018b, ApJL, 868, L33).
- Repeated **MR-CC** events are identified, suggesting that they are common phenomena in the solar corona (Li+ 2019, ApJ, 884, 34).
- **CR** formation mechanism by **MR-CC** can be used to explain some **CR** events with curved loop trajectories in the chromospheric and transition region channels (Li+ 2020, ApJ, 905, 26; Li+ 2021b, RAA, 21, 255).
- On-disk **MR-CC** events are investigated (Li+ 2021a, ApJ, 910, 82).
- **MR-CC** can be used to explain the supersonic downflows above the sunspot (Chen+ 2022, A&A, 659, A107).
- Filament formed by tether-cutting **MR** between loops and **CC** of chromospheric evaporated hot plasma are reported (Li+ 2021c, ApJL, 919, L21).

Thank you!